



# Applicability of Hill48 Yield Model and Effect of Anisotropic Parameter Determination Methods on Anisotropic Prediction

Zhenkai Mu, Jun Zhao, Qingdang Meng, Xueying Huang, and Gaochao Yu

Submitted: 18 May 2021 / Revised: 3 October 2021 / Accepted: 8 October 2021 / Published online: 15 November 2021

In this paper, the limitations of the Hill48 yield model in predicting directional yield stresses and plastic strain ratios ( $r$ -values) were investigated. According to a theoretical derivation, there are several inherent forms of the variation law of uniaxial tensile yield stress and  $r$ -value with angles calculated by Hill48. Three types of materials, DC04, DP600 and AA3104, were taken as research objects, and the anisotropic parameters and prediction errors were obtained by direct solution methods and the non-associated flow rule (non-AFR) methods based on different numbers of experimental data were analyzed. The results show that the prediction accuracy of the Hill48 yield model mainly depends on whether the anisotropic behavior of the material satisfies the above change law and is not directly related to the value of  $r$ . On this basis, under the associated flow rule, an anisotropic parameter identification method based on the conditional extremum of the cost function was proposed. It can significantly improve the prediction accuracy of low-carbon steel materials compared with the direct solution method. The research results provide detailed insight into the reasonable application of the Hill48 model in sheet metal forming and a reference for investigating the limitations of other advanced yield models.

**Keywords** constitutive model, parameter identification, plastic anisotropy, sheet metal forming

## 1. Introduction

Due to the influence of the rolling process, sheet metals usually exhibit anisotropic properties, which seriously affect the product formability and performance. Efforts have been made by researchers to develop constitutive models to predict the plastic anisotropy of sheet metals under various loading conditions. Hill (Ref 1) proposed the first yield model describing the anisotropy of orthotropic metal plates. However, this quadratic yield function has limited prediction accuracy for aluminum alloys. Barlat and Lian (Ref 2) extended the Hosford (Ref 3) model and proposed a non-quadratic yield criterion (Yld89) for materials with high planar anisotropy. Barlat et al. (Ref 4) extended the Yld89 yield criterion to a full stress state by introducing a linear transformation and proposed the Yld91 yield criterion. Later, a plane stress yield criterion using two linear transformations of the deviatoric stress tensor, referred to as Yld2000-2d, was proposed (Ref 5). Thereafter, Barlat et al. (Ref 6) developed the Yld2004-18p yield criterion, which was established for a pressure-independent material under general

stress conditions. Cazacu et al. (Ref 7) extended the work of Barlat et al. to hexagonal close-packed metals. Hu (Ref 8) proposed an anisotropic model that takes distortional anisotropy into account.

As the basis of an FE model, accurate constitutive relations and corresponding constitutive parameters are prerequisites for a successful simulation (Ref 9,10). When conventional analytical methods are used to determine the anisotropic parameters, many homogeneous tests with different loading paths are required to meet the basic condition: the number of tests is larger than the number of anisotropic parameters. Uniaxial tensile tests along different orientation angles from the rolling direction are typically used. For simple yield equations such as Hill48 and Yld91, the three uniaxial yield stresses and three  $r$ -values are sufficient. However, six experimental datasets are insufficient to calibrate the advanced yield criteria, which include at least seven anisotropic parameters (Ref 5). Thus, additional experimental data are needed, such as balanced biaxial stress by hydraulic bulging (Ref 11), balanced biaxial strain ratio (Ref 12), and plane strain (Ref 13). By combining the standard uniaxial tensile specimen and notched specimen, Bron and Besson (Ref 14) completed the parameter identification of the Bron-Besson yield criterion by changing the notch size to obtain different deformation paths. Due to the complexity of the high-order yield equation, with the increase in experimental data, the anisotropic parameters cannot be solved by analytical methods. Therefore, it is usually translated into a solution of minimizing the cost function, which determines the difference between the experimental results and the values calculated by the model (Ref 15).

In the conventional analytical approaches to anisotropic parameters, as explained earlier, a large number of homogeneous tests are time-consuming. In addition, the hydraulic bulge, biaxial tension, and shear tests require professional equipment, which is inconvenient. Therefore, Grytten et al.

Zhenkai Mu, Jun Zhao, Qingdang Meng, Xueying Huang, and Gaochao Yu, Key Laboratory of Advanced Forging & Stamping Technology and Science (Yanshan University), Ministry of Education of China, Qinhuangdao City 066004, People's Republic of China; and College of Mechanical Engineering, Yanshan University, Qinhuangdao City, People's Republic of China. Contact e-mails: mzk@stumail.yzu.edu.cn, zhaojun@ysu.edu.cn, mengqingdangysu@163.com, hxy@stumail.yzu.edu.cn, and gch\_yu@ysu.edu.cn.

(Ref 16) completed the parameter calibration of Yld2004-18p by replacing the experimental balanced biaxial stress and  $r$ -value with the calculated value using the Taylor model. Zhu et al. (Ref 17) determined the anisotropic parameters of Yld2000-2d by introducing a plane strain test instead of an equi-biaxial tensile test. The influence of different numbers and types of experimental results on the anisotropic parameters of different anisotropic yield models were analyzed by Khalfallah et al. (Ref 18) and Tang et al. (Ref 19). On this basis, the artificial data obtained from Yld91 were used to substitute the missing experimental data to identify the anisotropic parameters of CB2001, and the robustness of this method was also assessed (Ref 20). Hariharan et al. (Ref 21) proposed robust multi-objective optimization based on an evolutionary algorithm. This method can overcome the limitations in the approaches used before by minimizing the error in yield stress and plastic strain ratio simultaneously. Based on this method, the effects of experimental data on determining the coefficients of Hill48, Barlat 89 and Yld2000-2d were analyzed by Bandyopadhyay et al. (Ref 22), and the results indicated that there is a limit to the improvement of accuracy with the increase of the input experimental data.

With the development of computational methods and full-field deformation measurement technology, the identification of anisotropic parameters is no longer dependent on conventional experiments with homogeneous stress states (Ref 23). One of the widely applied inverse identification strategies is finite element model updating (FEMU). Based on this methodology, researchers have identified the anisotropic parameters of various yield criteria from notched specimen tensile tests (Ref 24) and heterogeneous biaxial tensile tests (Ref 25). Souto et al. (Ref 26) provided an optimization framework for designing heterogeneous specimens and determined the anisotropic parameters of the Yld2004-18p yield criterion with the designed heterogeneous test and the FEMU method. The other commonly used inverse method is the virtual fields' method (VFM). In this methodology, the full-field strain data are used to minimize the gap between the internal virtual work (IVW) and external virtual work (EVW) of the whole deformation process. The computational efficiency of this method is greatly improved as the iteration of FE model updating is skipped, particularly for advanced nonlinear anisotropic models. The application of the VFM to plasticity was first proposed by Grédiac and Pierron (Ref 27), and then Pierron et al. (Ref 28) extended it to cyclic loads and kinematic hardening. Later, Rossi and Pierron (Ref 29) first investigated the anisotropic plasticity based on the VFM, in which a complete three-dimensional framework for large-strain plasticity was presented. In addition, different heterogeneous stress states can be obtained by changing the structure and loading conditions of the specimens, such as tensile notched tests (Ref 30), unnotched Iosipescu tests (Ref 31),  $\Sigma$ -shaped specimens (Ref 32), and biaxially stretched cross-shaped specimens (Ref 33). Zhang et al. (Ref 34) compared the identification methods of the parameters of the Bron and Besson yield models based on conventional homogeneous tests and heterogeneous biaxial tensile tests. Fu et al. (Ref 35) proposed a novel method that enables the simultaneous identification of the multiple anisotropic yields and hardening constitutive parameters from a single test using the simplest uniaxial testing machine.

For both the traditional methods and the inverse methods, the basic strategy for improving the prediction accuracy of the

yield model is to increase the different types of experimental data so that the anisotropic parameters can contain more anisotropic properties. However, there are few investigations on the prediction limitations of the yield model itself. That is, the distribution of directional yield stress and  $r$ -values with respect to angle is the fundamental factor that determines whether the anisotropic yield model can achieve accurate prediction. Therefore, the limitations of the Hill48 yield model on the prediction of directional yield stress and  $r$ -values are analyzed in detail, and the comparison with the non-quadratic yield model Yld89 containing four anisotropic parameters is performed. Moreover, considering the application convenience and limitations of the Hill48 yield model, the conditional extremum method for identifying the anisotropic parameters is proposed. Then, a detailed implementation of each strategy, focusing on the input experimental data aspect, is presented, and their advantages and disadvantages are also discussed.

## 2. Yield Models

### 2.1 Hill48 Yield Model

The Hill48 yield model is an extension of the von Mises isotropic yield criterion to orthotropy and is defined as

$$2f(\sigma_{ij}) = F(\sigma_y - \sigma_z)^2 + G(\sigma_z - \sigma_x)^2 + H(\sigma_x - \sigma_y)^2 + 2L\tau_{yz}^2 + 2M\tau_{zx}^2 + 2N\tau_{xy}^2 = 1 \quad (\text{Eq 1})$$

where  $F$ ,  $G$ ,  $H$ ,  $L$ ,  $M$ , and  $N$  are the anisotropic parameters. Under plane stress state, there is

$$2f(\sigma_{ij}) = (G + H)\sigma_x^2 - 2H\sigma_x\sigma_y + (F + H)\sigma_y^2 + 2N\tau_{xy}^2 = 1 \quad (\text{Eq 2})$$

**2.1.1 Uniaxial Tensile Yield Stress.** The following relationship can be obtained based on the stress transformation of the uniaxial loading to the anisotropic axes.

$$\begin{cases} \sigma_x = \sigma_\alpha \cos^2 \alpha \\ \sigma_y = \sigma_\alpha \sin^2 \alpha \\ \tau_{xy} = \sigma_\alpha \sin \alpha \cos \alpha \end{cases} \quad (\text{Eq 3})$$

where  $\sigma_\alpha$  is the uniaxial tensile yield stress in direction  $\alpha$  with respect to the rolling direction. Substituting Eqs 3 into 2, the uniaxial tensile yield stress can be written as

$$\sigma_\alpha = \frac{1}{\sqrt{F \sin^2 \alpha + G \cos^2 \alpha + H + (2N - F - G - 4H) \sin^2 \alpha \cos^2 \alpha}} \quad (\text{Eq 4})$$

Let  $d\sigma_\alpha/d\alpha = 0$ ; thus,

$$2 \sin \alpha \cos \alpha [(F - G) + (2N - F - G - 4H)(1 - 2 \sin^2 \alpha)] = 0 \quad (\text{Eq 5})$$

It is obvious that the solutions of Eq 5 exist in  $\sin \alpha = 0$ ,  $\cos \alpha = 0$ , and  $(F - G) + (2N - F - G - 4H) \frac{1 - \tan^2 \alpha}{1 + \tan^2 \alpha} = 0$ .

Therefore, the distribution curve of the directional yield stress from 0° to 90° has at most three extreme points:  $\alpha=0$ ,  $\alpha=\pi/2$ , and  $\alpha=\bar{\alpha}=\tan^{-1}\sqrt{\frac{N-G-2H}{N-F-2H}}$ . Furthermore, by analyzing the second derivative of  $\sigma_\alpha$ , the following cases can be obtained. A schematic diagram of the various laws for directional yield stresses is given in Fig. 1(a).

- (1) When  $N$  is between  $F + 2H$  and  $G + 2H$ , there is no real value of  $\bar{\alpha}$ . If  $F < G$ , the uniaxial tensile yield stress exhibits a local minimum in the 0° direction and a local maximum in the 90° direction. The yield stress increases monotonically from 0° to 90° (S-Case 1); in contrast, if  $F > G$ , the yield stress decreases monotonically from 0° to 90° (S-Case 2).
- (2) When  $N > F + 2H$  and  $N > G + 2H$ , the uniaxial tensile yield stress exhibits local maximum values in the 0° and 90° directions, and there is a local minimum value in the  $\bar{\alpha}$  direction. Under this condition, the curve of directional stress versus angle is a unimodal function (S-Case 3).
- (3) When  $N < F + 2H$  and  $N < G + 2H$ , the uniaxial tensile yield stress exhibits local minimum values in the 0° and 90° directions, and there is a local maximum in the  $\bar{\alpha}$  direction. Under this condition, the curve of directional stress versus angle is a single valley function (S-Case 4).

**2.1.2  $r$ -values.** According to the Drucker flow rule, each component of the strain increment satisfies

$$\begin{cases} d\epsilon_x = [(G + H) \cos^2 \alpha - H \sin^2 \alpha] \sigma dc \\ d\epsilon_y = [(F + H) \sin^2 \alpha - H \cos^2 \alpha] \sigma dc \\ d\epsilon_z = -(F \sin^2 \alpha + G \cos^2 \alpha) \sigma dc \\ d\gamma_{xy} = (N \sin \alpha \cos \alpha) \sigma dc \end{cases} \quad (\text{Eq 6})$$

The uniaxial tensile transverse strain increment in the direction  $\alpha$  with respect to the rolling direction can be written as  $d\epsilon_{\alpha+\pi/2} = d\epsilon_x \sin^2 \alpha + d\epsilon_y \cos^2 \alpha - 2d\gamma_{xy} \sin \alpha \cos \alpha$  (Eq 7)

Substituting Eq 6 into Eq 7, the ratio of the transverse strain increment to the thickness strain increment can be obtained as

$$r_\alpha = \frac{d\epsilon_{\alpha+\pi/2}}{d\epsilon_z} = \frac{H + (2N - F - G - 4H) \sin^2 \alpha \cos^2 \alpha}{F \sin^2 \alpha + G \cos^2 \alpha} \quad (\text{Eq 8})$$

Let  $\frac{dr_\alpha}{d\alpha} = \frac{dr_\alpha}{d \sin^2 \alpha} \frac{d \sin^2 \alpha}{d\alpha} = 0$ ; thus,

$$2 \sin \alpha \cos \alpha \{ (2N - F - G - 4H)(F \sin^2 \alpha + G \cos^2 \alpha)(\cos^2 \alpha - \sin^2 \alpha) - [H + (2N - F - G - 4H) \sin^2 \alpha \cos^2 \alpha](F - G) \} = 0 \quad (\text{Eq 9})$$

It is obvious that  $\alpha=0$  and  $\alpha=\pi/2$  are the two solutions of Eq 9. Other solutions  $\alpha=\bar{\alpha}$  exist in the following equation.

$$(2N - F - G - 4H)(F \sin^2 \alpha + G \cos^2 \alpha)(\cos^2 \alpha - \sin^2 \alpha) - [H + (2N - F - G - 4H) \sin^2 \alpha \cos^2 \alpha](F - G) = 0 \quad (\text{Eq 10})$$

According to Eq 10, there is

$$\sin^2 \bar{\alpha} = G \left/ (G - F) \pm \sqrt{GF / (G - F)^2 - H / (2N - F - G - 4H)} \right. \quad (\text{Eq 11})$$

Let

$$\begin{cases} K_1 = G \left/ (G - F) + \sqrt{GF / (G - F)^2 - H / (2N - F - G - 4H)} \right. \\ K_2 = G \left/ (G - F) - \sqrt{GF / (G - F)^2 - H / (2N - F - G - 4H)} \right. \end{cases} \quad (\text{Eq 12})$$

A schematic diagram of the various laws for the  $r$ -value is given in Fig. 1(b).

- (1) When  $0 < K_1 < 1$ ,  $|K_2| > 1$  or  $0 < K_2 < 1$ ,  $|K_1| > 1$ , there is one real value of  $\bar{\alpha}$ . The  $r$ -values are extremum in the 0°,  $\bar{\alpha}$ , and 90° directions. Under this condition, the curve of  $r$ -values versus angle is a single valley function ( $r$ -Case 1) or unimodal function ( $r$ -Case 2).
- (2) When  $|K_1| > 1$  and  $|K_2| > 1$ , there is no real value of  $\bar{\alpha}$ . The  $r$ -values are extremum in the 0° and 90° directions.

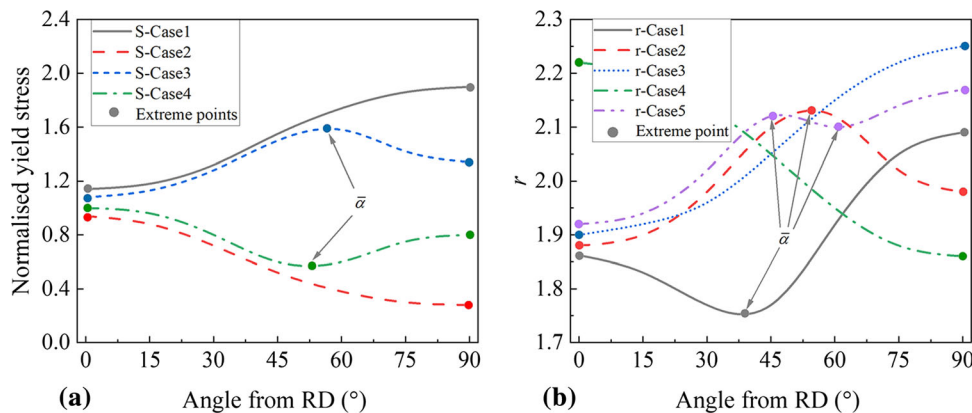


**Fig. 1** Schematic of the distribution law for (a) uniaxial tensile yield stress and (b)  $r$ -value

Under this condition, the  $r$ -values increase or decrease monotonically with the change in  $\alpha$  ( $r$ -Case 3 and  $r$ -Case 4).

- (3) When  $0 < K_1 < 1$  and  $0 < K_2 < 1$ , there are two real values of  $\bar{\alpha}$ . The  $r$ -values are extremum in the  $0^\circ$ ,  $\bar{\alpha}_1$ ,  $\bar{\alpha}_2$  and  $90^\circ$  directions. Under this condition, the curve of  $r$ -values versus angle coexists as a peak and a valley ( $r$ -Case 5). If there is a local maximum in the  $0^\circ$  direction, there is a local minimum in the  $90^\circ$  direction; in contrast, if there is a local minimum in the  $0^\circ$  direction, there is a local maximum in the  $90^\circ$  direction.

According to the above analysis, the Hill48 yield model has several inherent forms for predicting the uniaxial tensile yield stress and  $r$ -value. In other words, when the anisotropic behavior of the material approximately satisfies the above situations, it is possible to obtain relatively accurate prediction results according to the Hill48 yield model. Otherwise, it can be expected that the predicted results will deviate from the experimental results to a great extent.

## 2.2 Yld89 Yield Model

The Hill48 yield model is considered to be satisfactory for steel but cannot accurately describe the anisotropy of aluminum alloy materials. For this, Barlat and Lian (Ref 2) extended the Hosford isotropic yield criterion based on crystallography to in-plane anisotropy and proposed the Yld89 yield model.

$$\Phi = a|K_1 + K_2|^m + a|K_1 - K_2|^m + c|2K_2|^m = 2\bar{\sigma}^m \quad (\text{Eq 13})$$

$$K_1 = \frac{\sigma_{xx} + h\sigma_{yy}}{2}, K_2 = \sqrt{\left(\frac{\sigma_{xx} - h\sigma_{yy}}{2}\right)^2 + (p\sigma_{xy})^2} \quad (\text{Eq 14})$$

where  $m$  is the exponent of the yield function and is recommended as 6 for BCC and 8 for FCC polycrystals. The coefficients  $a$ ,  $c$ ,  $h$  and  $p$  are the anisotropic parameters, which can be calculated based on either  $r$ -values or yield stresses.

The uniaxial yield stress and  $r$ -value along an arbitrary orientation can be given as

$$\sigma_\alpha = \bar{\sigma} \left[ \frac{2}{aS_1^m + aS_2^m + c(S_1 - S_2)^m} \right]^{1/m} \quad (\text{Eq 15})$$

$$r_\alpha = \frac{2m\bar{\sigma}^m}{\left(\frac{\partial\Phi}{\partial\sigma_{xx}} + \frac{\partial\Phi}{\partial\sigma_{yy}}\right)\sigma_\alpha} - 1 \quad (\text{Eq 16})$$

where

$$S_1, S_2 = \frac{\cos^2 \alpha + h \sin^2 \alpha}{2} \pm \sqrt{\left(\frac{\cos^2 \alpha - h \sin^2 \alpha}{2}\right)^2 + p^2 \cos^2 \alpha \sin^2 \alpha} \quad (\text{Eq 17})$$

The equi-biaxial yield stress and  $r$ -value can be expressed as

$$\sigma_b = \bar{\sigma} \left[ \frac{2}{a + ah^m + c(1-h)^m} \right]^{1/m} \quad (\text{Eq 18})$$

$$r_b = \frac{\partial\Phi}{\partial\sigma_{yy}} / \frac{\partial\Phi}{\partial\sigma_{xx}} \quad (\text{Eq 19})$$

## 3. Effect of Parameter Identification Methods and Experimental Data on Anisotropic Prediction

### 3.1 Material Properties

To further provide detailed insight into the limitations of the Hill48 yield model in predicting uniaxial tensile yield stress,  $r$ -values and yield loci, low-carbon steel, aluminum alloy and high-strength steel with obvious differences in the distribution of uniaxial tensile yield stress and  $r$ -values are selected as the research objects, and the experimental data for uniaxial tension are shown in Table 1.

### 3.2 Prediction Based on Direct Solution Methods (DS Methods)

Uniaxial tensile tests in orientations of  $0^\circ$ ,  $45^\circ$ , and  $90^\circ$  are commonly carried out. Therefore, the experimental uniaxial tensile yield stresses and  $r$ -values along these three orientations are commonly used to calculate the anisotropic parameters of the yield model. According to the Hill48 yield model, the following system of equations can be obtained:

$$\begin{cases} \sigma_0^2 = \frac{1}{G+H} & r_0 = \frac{H}{G} \\ \sigma_{45}^2 = \frac{4}{F+G+2N} & r_{45} = \frac{1}{2} \left( \frac{2N}{F+G} - 1 \right) \\ \sigma_{90}^2 = \frac{1}{F+H} & r_{90} = \frac{H}{F} \end{cases} \quad (\text{Eq 20})$$

For Yld89 yield model, when  $\bar{\sigma} = \sigma_0$ , there is

$$\begin{cases} \sigma_0 = \sigma_0 \left( \frac{2}{a+c} \right)^{1/m} & r_0 = \frac{2}{a+c(1-h)} - 1 \\ \sigma_{45} = \sigma_0 \left[ \frac{2}{aS_1^m + aS_2^m + c(S_1 - S_2)^m} \right]^{1/m} & r_{45} = \frac{2m\bar{\sigma}_0^m}{(\partial\Phi/\partial\sigma_{xx} + \partial\Phi/\partial\sigma_{yy})\sigma_{45}} - 1 \\ \sigma_{90} = \frac{\sigma_0}{h} \left( \frac{2}{a+c} \right)^{1/m} & r_{90} = \frac{2(\sigma_0/\sigma_{90})^m}{[-c + (a+c)h]h^{m-1}} - 1 \end{cases} \quad (\text{Eq 21})$$

The above system of equations is overdetermined equations. Different solutions can be obtained by different sets of experimental data. Parameter  $N$  of Hill48 and  $p$  of Yld89 are only related to  $\sigma_{45}$  and  $r_{45}$ . Therefore, at least one of  $\sigma_{45}$  and  $r_{45}$  should be included. Eight typical sets of experimental data are shown in Table 2. The anisotropic parameters of these materials calculated based on different sets of experimental data are shown in Appendix Table 3. The predicted uniaxial tensile yield stresses and  $r$ -values based on the different DS methods are shown in Fig. 2.

To more clearly show the prediction error distribution in different directions obtained by different methods, the relative errors of the directional yield stresses  $\zeta_\alpha^\sigma$  and  $r$ -values  $\zeta_\alpha^r$  in different directions are calculated by Eq 22, as shown in Fig. 3.

$$\zeta_\alpha^\sigma = \frac{|\sigma_\alpha^{\text{pre}} - \sigma_\alpha^{\text{exp}}|}{\sigma_\alpha^{\text{exp}}}, \zeta_\alpha^r = \frac{|r_\alpha^{\text{pre}} - r_\alpha^{\text{exp}}|}{r_\alpha^{\text{exp}}} \quad (\text{Eq 22})$$

where  $\sigma_\alpha^{\text{exp}}$  and  $r_\alpha^{\text{exp}}$  are the experimental directional yield stresses and  $r$ -values at a particular orientation  $\alpha$  with respect to

**Table 1 Experimental data for uniaxial tension**

Angle from RD (°)	DC04		DP600		AA3104	
	<i>r</i> -values	Initial yield stress	<i>r</i> -values	Initial yield stress	<i>r</i> -values	Initial yield stress
0	1.862	135.57	0.94	419.40	0.403	281.15
15	1.812	136.39	0.92	426.80	0.413	285.79
30	1.726	139.18	1.13	432.70	0.557	286.97
45	1.741	142.61	1.44	436.00	0.888	286.41
60	1.918	143.85	1.15	455.20	0.927	293.50
75	2.162	141.92	1.00	463.80	1.060	297.71
90	2.353	140.61	0.90	467.30	1.125	294.69
Biaxial	0.82	137.19	0.80	408.40	0.783	326.60

**Table 2 Direct solution methods based on different sets of experimental data**

Methods	$\sigma_0$	$\sigma_{45}$	$\sigma_{90}$	$r_0$	$r_{45}$	$r_{90}$
DS1	✓	✓	✓	✓		
DS2	✓	✓	✓			✓
DS3	✓	✓		✓		✓
DS4		✓	✓	✓		✓
DS5	✓		✓	✓	✓	
DS6	✓		✓		✓	✓
DS7	✓			✓	✓	✓
DS8			✓	✓	✓	✓

RD, respectively.  $\sigma_{\alpha}^{pre}$  and  $r_{\alpha}^{pre}$  are the corresponding predictions based on the yield model.

For the DC04 material, the change law of the uniaxial tensile yield stresses and *r*-values approximately satisfy the form predicted by the Hill48 yield model. Therefore, the DS methods based on different experimental data can capture their change laws of yield stresses and *r*-values. The differences between these DS methods are mainly caused by  $\sigma_{45}$  and  $r_{45}$ , while other experimental data have little effect on the results, as shown in Fig. 2. For the DP600 and AA3104 materials, it is obvious that the distribution forms of the uniaxial tensile yield stresses and *r*-values do not meet the change laws predicted by the Hill48 yield model. Therefore, the prediction errors of DS methods are relatively large, and there are

**Table 3 Anisotropic parameters obtained by different DS methods**

Materials		DS1	DS2	DS3	DS4	DS5	DS6	DS7	DS8
DC04	<i>H</i>	3.54E-05	3.55E-05	3.54E-05	3.55E-05	3.54E-05	3.55E-05	3.54E-05	3.55E-05
	<i>F</i>	1.52E-05	1.51E-05	1.5E-05	1.51E-05	1.52E-05	1.51E-05	1.5E-05	1.51E-05
	<i>G</i>	1.9E-05	1.89E-05	1.9E-05	1.91E-05	1.9E-05	1.89E-05	1.9E-05	1.91E-05
	<i>N</i>	8.12E-05	8.13E-05	8.13E-05	8.13E-05	7.66E-05	7.62E-05	7.63E-05	7.65E-05
	<i>a</i>	0.650	0.647	0.649	0.654	0.650	0.647	0.649	0.654
	<i>c</i>	1.350	1.353	1.351	1.363	1.350	1.353	1.351	1.363
	<i>h</i>	0.964	0.964	0.963	0.963	0.964	0.964	0.963	0.963
	<i>p</i>	0.944	0.944	0.944	0.943	0.938	0.936	0.937	0.937
	<i>m</i>	6.000	6.000	6.000	6.000	6.000	6.000	6.000	6.000
	DP600	<i>H</i>	2.75E-06	2.16E-06	2.75E-06	2.16E-06	2.75E-06	2.16E-06	2.75E-06
<i>F</i>		1.82E-06	2.41E-06	3.06E-06	2.41E-06	1.82E-06	2.41E-06	3.06E-06	2.41E-06
<i>G</i>		2.93E-06	3.52E-06	2.93E-06	2.30E-06	2.93E-06	3.51E-06	2.93E-06	2.30E-06
<i>N</i>		8.14E-06	7.56E-06	7.52E-06	8.16E-06	9.22E-06	1.14E-05	1.16E-05	9.15E-06
<i>a</i>		0.920	1.150	1.042	0.509	0.920	1.150	1.042	0.509
<i>c</i>		1.080	0.850	0.958	0.468	1.080	0.850	0.958	0.468
<i>h</i>		0.897	0.897	1.011	1.011	0.897	0.897	1.011	1.011
<i>p</i>		0.964	0.966	0.946	1.109	1.004	1.135	1.132	1.132
<i>m</i>		6.000	6.000	6.000	6.000	6.000	6.000	6.000	6.000
AA3104		<i>H</i>	3.63E-06	6.10E-06	3.63E-06	6.10E-06	3.63E-06	6.10E-06	3.63E-06
	<i>F</i>	7.88E-06	5.42E-06	3.23E-06	5.42E-06	7.88E-06	5.42E-06	3.23E-06	5.42E-06
	<i>G</i>	9.02E-06	6.55E-06	9.02E-06	1.51E-05	9.02E-06	6.55E-06	9.02E-06	1.51E-05
	<i>N</i>	1.59E-05	1.84E-05	1.83E-05	1.41E-05	2.35E-05	1.66E-05	1.70E-05	2.85E-05
	<i>a</i>	1.398	0.990	1.220	9.664	1.398	0.990	1.220	9.664
	<i>c</i>	0.602	1.010	0.780	6.178	0.602	1.010	0.780	6.178
	<i>h</i>	0.954	0.954	0.737	0.737	0.954	0.954	0.737	0.737
	<i>p</i>	0.984	0.983	1.015	0.686	1.129	0.951	0.940	0.940
	<i>m</i>	8.000	8.000	8.000	8.000	8.000	8.000	8.000	8.000

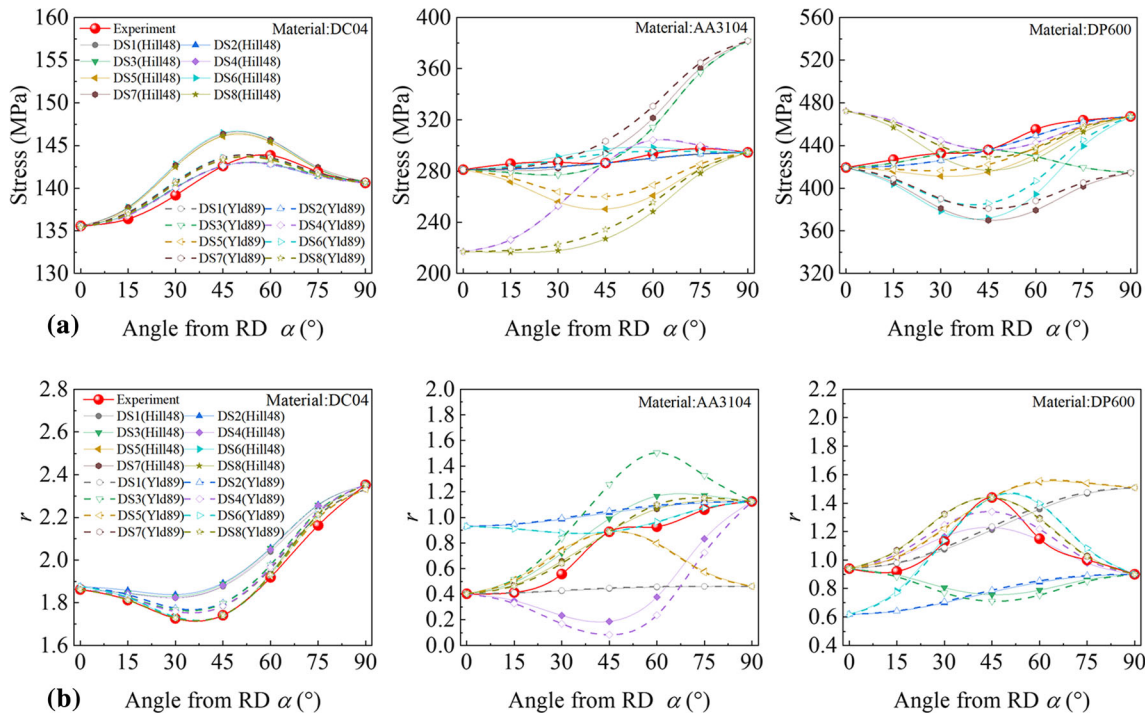


**Fig. 2** Comparison between experimental data and the results predicted by different DS methods: (a) Directional yield stresses; (b)  $r$ -values

also large differences between different sets of experimental data. These phenomena can also be found in the prediction results of the Yld89 yield model. Compared with the Hill48 yield model, the predicted results of the Yld89 yield model are closer to the experimental results, especially for DC04.

The predicted yield loci in the normalized principal stress space are plotted in Fig. 4. According to these eight DS methods, as shown in Table 1, only four kinds of yield loci were obtained. That is, the yield loci obtained by DS1, DS2, DS3, and DS4 are equal to those of DS5, DS6, DS7, and DS8, respectively. Because the experimental equal-biaxial tensile yield stress is not included in the DS methods, the prediction of the equal-biaxial tensile yield stress is poor. Moreover, the yield loci of DC04 predicted by different DS methods are almost the same. However, there were obvious differences in the yield loci of AA3104 and DP600 predicted by these DS methods. This is mainly related to the degree of in-plane anisotropy and the variation of the uniaxial tensile yield stress and  $r$ -values with angle. The total prediction error under different stress states is calculated by Eq 23 and shown in Fig. 5.

$$\Omega = \zeta_{\sigma} + \zeta_r + \zeta_{\sigma b} + \zeta_{rb} \quad (\text{Eq 23})$$

where  $\zeta_{\sigma}$  and  $\zeta_r$  are the sum of prediction errors of the uniaxial tensile yield stresses and  $r$ -values at seven orientations, respectively.  $\zeta_{\sigma b}$  and  $\zeta_{rb}$  are the prediction errors of the equi-biaxial yield stress and  $r$ -value, respectively.

$$\zeta_{\sigma b} = \frac{|\sigma_b^{\text{pre}} - \sigma_b^{\text{exp}}|}{\sigma_b^{\text{exp}}}, \quad \zeta_{rb} = \frac{|r_b^{\text{pre}} - r_b^{\text{exp}}|}{r_b^{\text{exp}}} \quad (\text{Eq 24})$$

$$\zeta_{\sigma} = \sum_{i=1}^7 \frac{|\sigma_{\alpha_i}^{\text{pre}} - \sigma_{\alpha_i}^{\text{exp}}|}{\sigma_{\alpha_i}^{\text{exp}}}, \quad \zeta_r = \sum_{i=1}^7 \frac{|r_{\alpha_i}^{\text{pre}} - r_{\alpha_i}^{\text{exp}}|}{r_{\alpha_i}^{\text{exp}}} \quad (\text{Eq 25})$$

The DS methods cannot accurately predict directional stresses and  $r$ -values simultaneously. The main reason is that this method can only contain limited experimental data, which is not enough to fully reflect the anisotropic characteristics.

### 3.3 Solution Method Based on the Non-Associated Flow Rule (NA Methods)

In the non-associated flow rule (non-AFR), two independent functions of yield  $\bar{\sigma}_y(\sigma_{ij})$  and plastic potential  $\bar{\sigma}_p(\sigma_{ij})$  are used to determine the yield and plastic flow direction, respectively. For the Hill48 yield model, there is

$$\bar{\sigma}_y(\sigma_{ij}) = \sqrt{\frac{3}{2}} \left[ \frac{F_{\sigma} \sigma_y^2 + G_{\sigma} \sigma_x^2 + H_{\sigma} (\sigma_x - \sigma_y)^2 + 2N_{\sigma} \tau_{xy}^2}{F_{\sigma} + G_{\sigma} + H_{\sigma}} \right]^{\frac{1}{2}} \quad (\text{Eq 26})$$

$$\bar{\sigma}_p(\sigma_{ij}) = \sqrt{\frac{3}{2}} \left[ \frac{F_r \sigma_y^2 + G_r \sigma_x^2 + H_r (\sigma_x - \sigma_y)^2 + 2N_r \tau_{xy}^2}{F_r + G_r + H_r} \right]^{\frac{1}{2}} \quad (\text{Eq 27})$$

where  $F_{\sigma}$ ,  $G_{\sigma}$ ,  $H_{\sigma}$ , and  $N_{\sigma}$  are the parameters based on yield stresses, and  $F_r$ ,  $G_r$ ,  $H_r$ , and  $N_r$  are the parameters based on  $r$ -values. At present, the following equations are usually used to determine the stress-based anisotropic parameters and deformation anisotropic parameters.

$$\begin{cases} F_{\sigma} = \frac{1}{2} \left[ \frac{1}{\sigma_{90}^2} - \frac{1}{\sigma_0^2} + \frac{1}{\sigma_b^2} \right] & G_{\sigma} = \frac{1}{2} \left[ \frac{1}{\sigma_0^2} - \frac{1}{\sigma_{90}^2} + \frac{1}{\sigma_b^2} \right] \\ H_{\sigma} = \frac{1}{2} \left[ \frac{1}{\sigma_0^2} + \frac{1}{\sigma_{90}^2} - \frac{1}{\sigma_b^2} \right] & N_{\sigma} = \frac{1}{2} \left[ \frac{4}{\sigma_{45}^2} - \frac{1}{\sigma_b^2} \right] \end{cases} \quad (\text{Eq 28})$$

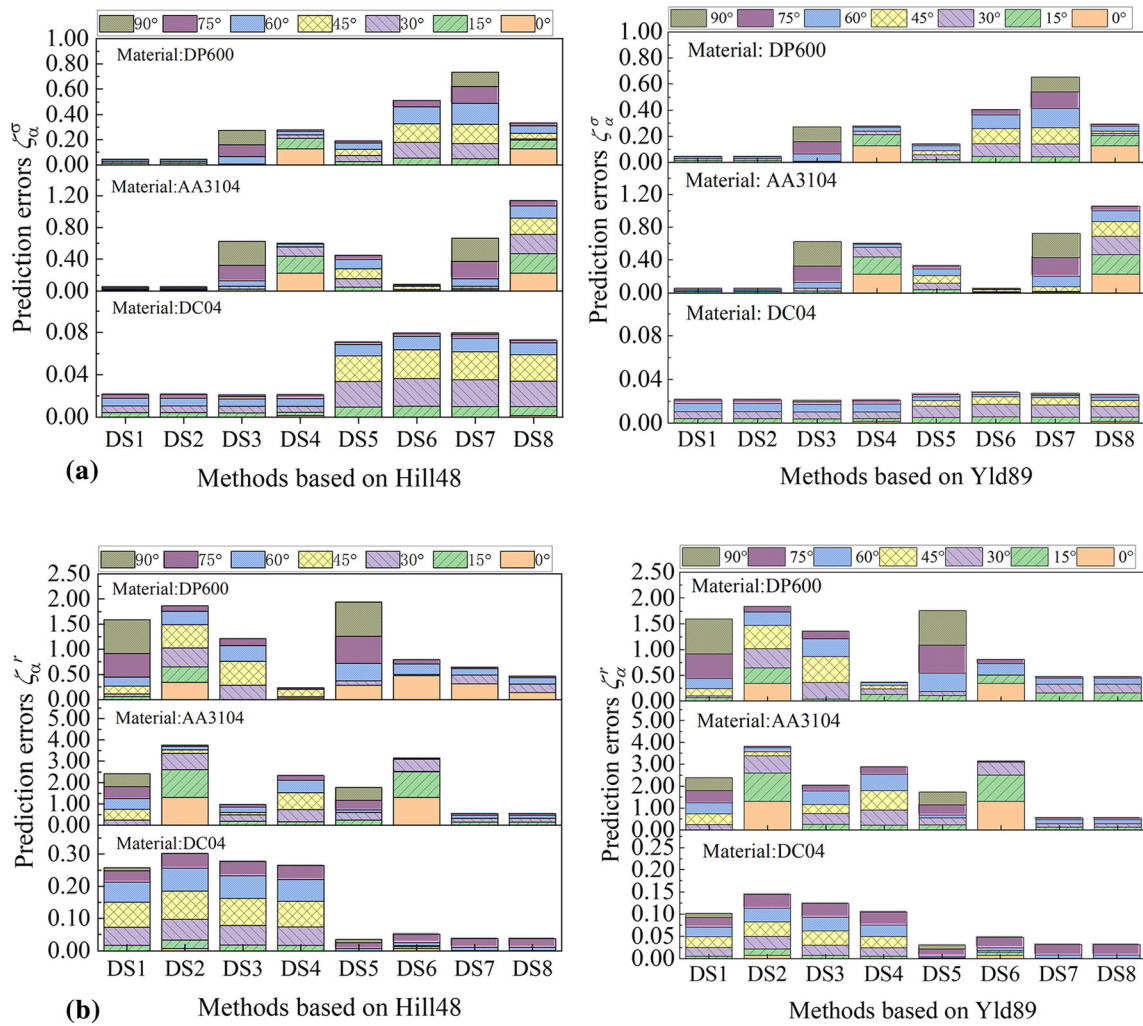


**Fig. 3** Prediction errors of uniaxial tension obtained by different DS methods (a) Directional yield stresses and (b)  $r$ -values at seven orientations

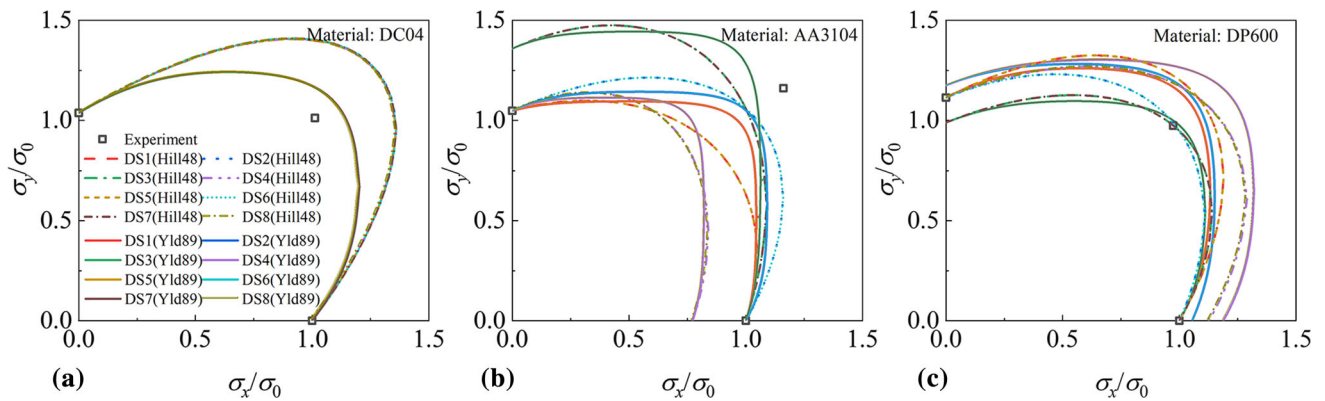


**Fig. 4** Predicted yield loci in the normalized principal stress space based on different DS methods

$$\begin{cases} F_r = \frac{r_0}{r_{90}(1+r_0)} & G_r = \frac{1}{(1+r_0)} \\ H_r = \frac{r_0}{(1+r_0)} & N_r = \frac{1}{2} \frac{(r_0+r_{90})(1+r_{45})}{r_{90}(1+r_0)} \end{cases} \quad (\text{Eq 29})$$

For the Yld89 yield model, the anisotropic parameters based on stress and  $r$ -values are calculated by Eqs 30 and 31, respectively. The anisotropic parameter  $p$  needs to be solved numerically.

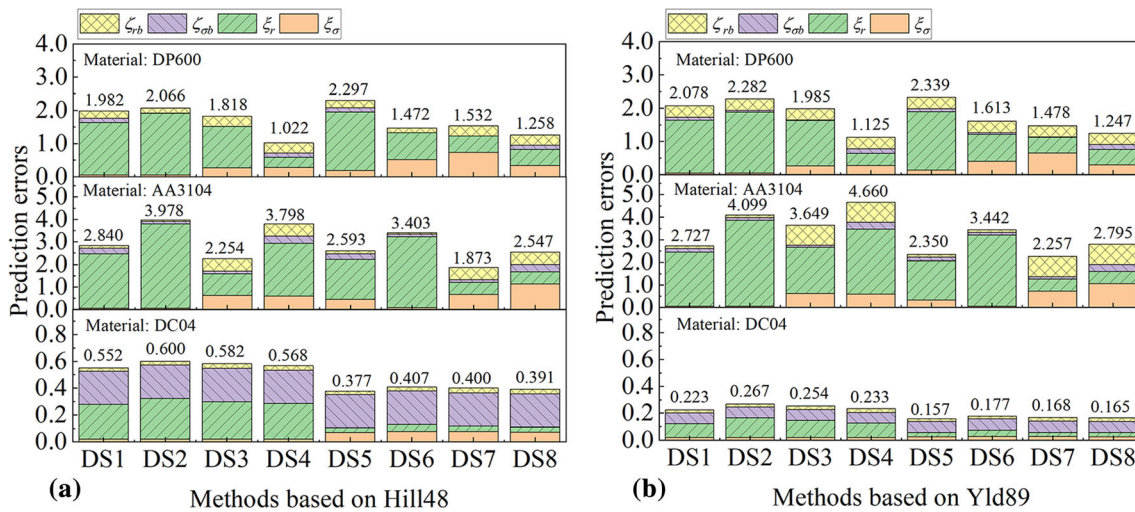


Fig. 5 Prediction errors under different stress states obtained by different DS methods

$$\begin{cases} c_{\sigma} = 2 - a_{\sigma} & \sigma_{45} = \sigma_0 \left[ \frac{2}{aS_1^m + aS_2^m + c(S_1 - S_2)^m} \right]^{1/m} \\ h_{\sigma} = \frac{\sigma_0}{\sigma_{90}} & a_{\sigma} = 2 \left[ \frac{(\sigma_0/\sigma_b)^m - (1-h)^m}{1+h^m - (1-h)^m} \right] \end{cases} \quad (\text{Eq 30})$$

$$\begin{cases} a_r = 2 - c_r & r_{45} = \frac{2m\bar{\sigma}_0^m}{(\partial\Phi/\partial\sigma_{xx} + \partial\Phi/\partial\sigma_{yy})\sigma_{45}} - 1 \\ h_r = \sqrt{\frac{r_0(1+r_{90})}{r_{90}(1+r_0)}} & c_r = 2\sqrt{\frac{r_0r_{90}}{(1+r_{90})(1+r_0)}} \end{cases} \quad (\text{Eq 31})$$

where  $\sigma_0$ ,  $\sigma_{45}$ , and  $\sigma_{90}$  are the experimental yield stresses at  $0^\circ$ ,  $45^\circ$ , and  $90^\circ$  with respect to RD, respectively.  $\sigma_b$  is the equi-biaxial yield stress.  $r_0$ ,  $r_{45}$ , and  $r_{90}$  are the experimental  $r$ -values obtained from the uniaxial tensile test at  $0^\circ$ ,  $45^\circ$ , and  $90^\circ$  with respect to RD, respectively. The method based on stress ( $\sigma_0$ ,  $\sigma_{45}$ ,  $\sigma_{90}$  and  $\sigma_b$ ) is named NAS1, and the method based on  $r$ -values ( $\sigma_0$ ,  $r_0$ ,  $r_{45}$  and  $r_{90}$ ) is named NAR1.

On this basis, cost function methods based on non-AFR are used to analyze the influence of the input experimental data on the prediction accuracy. The stress cost function and  $r$ -value cost function are constructed to solve the stress anisotropic parameters and deformation anisotropic parameters, respectively. As shown in the Eqs 32 and 33,

$$\Phi_{\sigma} = \sum_{i=1}^n \left[ \frac{(\sigma_{\alpha_i}^{\text{exp}})^2}{(\sigma_{\alpha_i}^{\text{pre}})^2} - 1 \right]^2 \quad (\text{Eq 32})$$

$$\Phi_r = \sum_{i=1}^n \left[ \frac{r_{\alpha_i}^{\text{exp}}}{r_{\alpha_i}^{\text{pre}}} - 1 \right]^2 \quad (\text{Eq 33})$$

where  $\sigma_{\alpha_i}^{\text{exp}}$  and  $r_{\alpha_i}^{\text{exp}}$  are the experimental directional yield stresses and  $r$ -values.  $\sigma_{\alpha_i}^{\text{pre}}$  and  $r_{\alpha_i}^{\text{pre}}$  are the corresponding prediction values calculated by the yield model.  $n$  is the number of experimental data points used in the cost function. When  $n = 4$ ,  $\alpha_1 = 0$ ,  $\alpha_2 = 30$ ,  $\alpha_3 = 60$ , and  $\alpha_4 = 90$ . Under this

condition, the stress cost function and  $r$ -value cost function are named NAS2 and NAR2, respectively. When  $n = 5$ ,  $\alpha_1 = 0$ ,  $\alpha_2 = 30$ ,  $\alpha_3 = 45$ ,  $\alpha_4 = 60$ , and  $\alpha_5 = 90$ . Under this condition, the stress cost function and  $r$ -value cost function are named NAS3 and NAR3, respectively. When  $n = 7$ ,  $\alpha_1 = 0$ ,  $\alpha_2 = 15$ ,  $\alpha_3 = 30$ ,  $\alpha_4 = 45$ ,  $\alpha_5 = 60$ ,  $\alpha_6 = 75$ , and  $\alpha_7 = 90$ . Under this condition, the stress cost function and  $r$ -value cost function are named NAS4 and NAR4, respectively. The anisotropic parameters can be determined by minimizing the cost function, as shown in Appendix Tables 4 and 5. The comparison of the predicted yield stresses and  $r$ -values with experimental data is shown in Fig. 6.

Compared with the DS methods, the prediction accuracy of non-AFR methods has been greatly improved. The results obtained by the different non-AFR methods are relatively small, especially for DC04. For material DC04, the increase in the number of experimental data used in the cost function will not improve the prediction accuracy. Therefore, for this kind of material, the basic experimental data are sufficient. Due to the limitations of the Hill48 yield model, it can only approximately predict the change law of directional stresses and  $r$ -values of DP600 and AA3104 materials with a monotonic function or unimodal function and cannot reflect their real change law. With the increase in the number of uniaxial tensile experimental data, the prediction curve is interspersed between the experimental points. The relative errors at seven orientations obtained by NAS3/NAR3 and NAS4/NAR4 are relatively uniform, but the accuracy is not notably improved, as shown in Fig. 9.

To investigate the effect of equi-biaxial tensile experimental data on the prediction results, the equi-biaxial tensile yield stress and  $r$ -value are added to the stress cost function and  $r$ -value cost function, respectively. The predicted uniaxial tensile yield stress and  $r$ -value based on the NA(EQ) methods (considering equi-biaxial tensile experimental data) are shown in Fig. 7. To distinguish these methods from the above methods, the stress-based methods are renamed NAS2(EQ), NAS3(EQ) and NAS4(EQ). The  $r$ -value-based methods are renamed NAR2(EQ), NAR3(EQ) and NAR4(EQ).

As shown in Fig. 7, when the equi-biaxial tensile experimental data are considered, the prediction accuracy of the uniaxial tensile yield stress of DC04 and the uniaxial tensile  $r$ -value of AA3104 obtained by the Hill48 yield model is



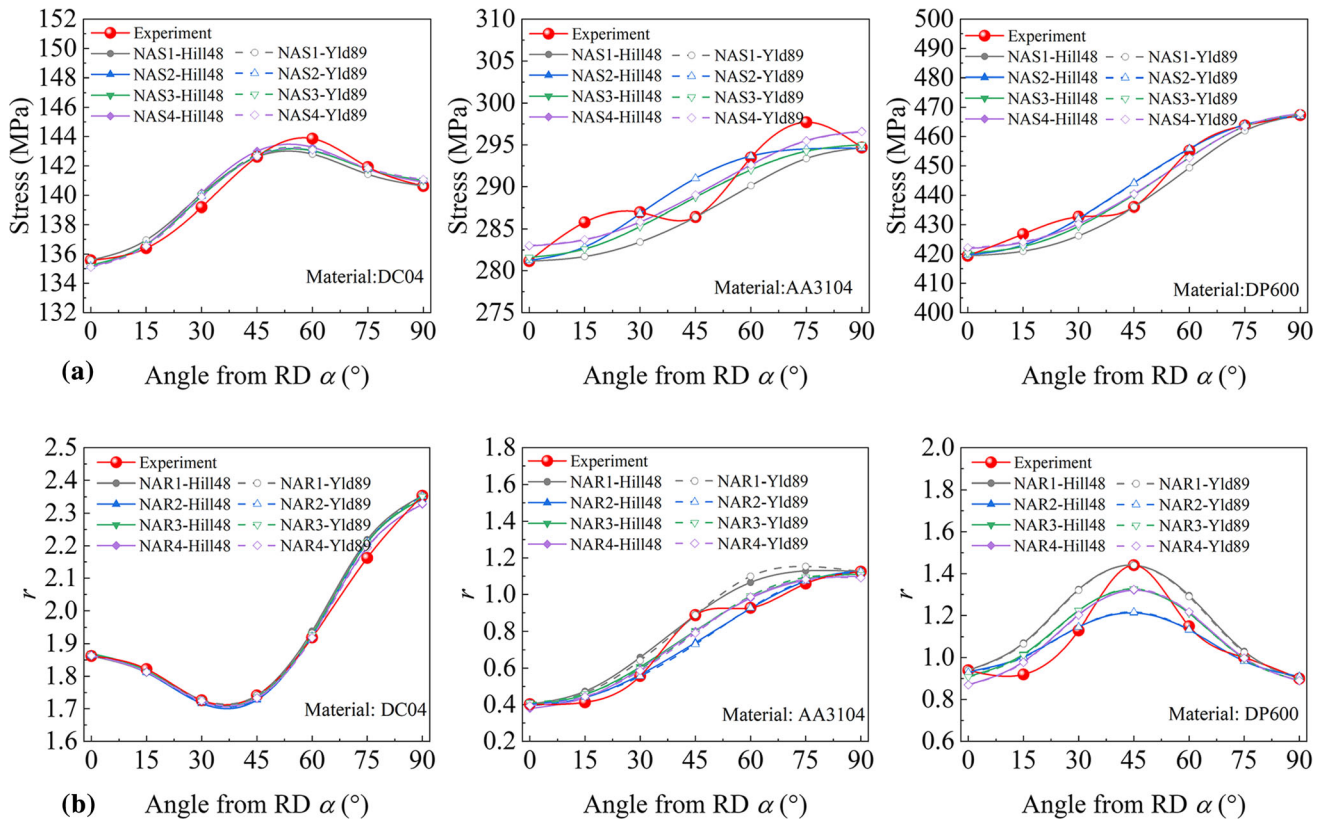


**Fig. 6** Comparison between experimental data and the results predicted by different NA methods (without equi-biaxial tensile experimental data): (a) Directional yield stresses; (b)  $r$ -values

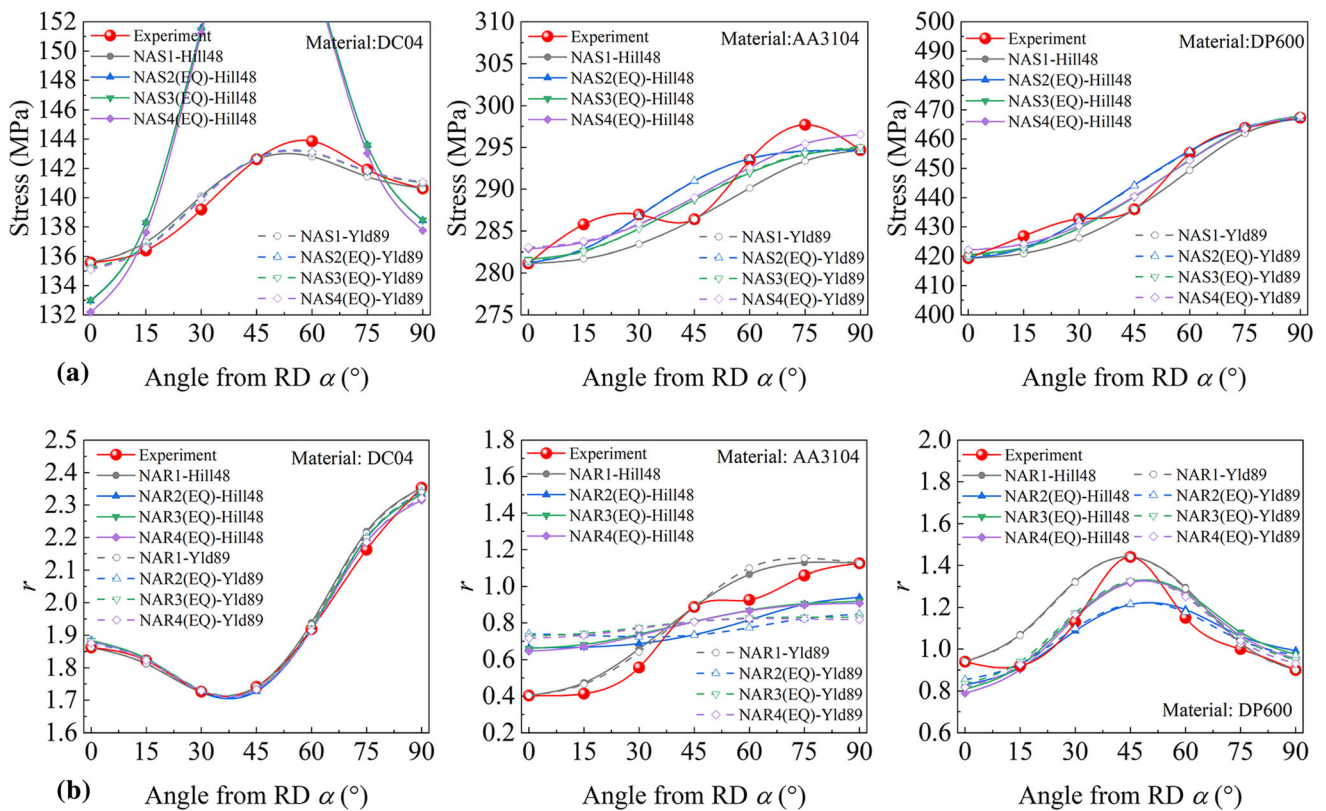


**Fig. 7** Comparison between experimental data and the results predicted by different NA(EQ) methods (containing equi-biaxial tensile experimental data): (a) Directional yield stresses; (b)  $r$ -values

significantly reduced. For the Yld89 yield model, this change is reflected only in the uniaxial tensile  $r$ -value of AA3104. A comparison between the yield loci predicted by different NAS methods (without equi-biaxial tensile stress) and those predicted by the NAS(EQ) methods (containing equi-biaxial tensile stress) is shown in Fig. 8. Different combinations of uniaxial tensile test data have a great impact on the NAS methods, and they cannot accurately capture the equi-biaxial tensile yield stress. When the equi-biaxial tensile yield stress is considered in the cost function, the influence of different uniaxial tensile test data on the yield locus can be ignored.

Figures 9 and 10 shows the total prediction errors obtained by different NA methods based on the Hill48 yield model and Yld89 yield model, respectively. For the Hill48 yield model, considering the equi-biaxial tensile experimental data cannot always effectively improve the total prediction accuracy, such as DC04 and AA3104. Although the prediction accuracy of equal-biaxial tensile stress and  $r$ -value has been improved by considering the equi-biaxial tensile experimental data in the cost function, it is not enough to offset the increased prediction error of uniaxial tension. The same law also occurs in the prediction results of the Yld89 yield model. Compared with the Hill48 yield model, it is helpful to consider the equi-biaxial tensile stress in the stress cost function to improve the stress prediction accuracy of the Yld89 yield model.

For different materials, appropriate solutions should be chosen. For materials whose changes law of the directional yield stresses and  $r$ -values approximately satisfy the predicted forms of the Hill48 yield model, the NA1 method can achieve good prediction accuracy under conventional experimental data. However, for aluminum alloys and high-strength steel

with a multipeak distribution of stress and  $r$ -values, the NA2 method is the best choice to approximately describe the uniaxial tensile yield stress and  $r$ -values.

However, the use of non-AFR requires a secondary development, which is inconvenient to the application. In addition, a large number of studies have shown that the anisotropic parameters based on the stress can only describe the yield stress well, and there are great errors in the prediction of  $r$ -values. The anisotropic parameters based on the  $r$ -values are the opposite. For this reason, under the associated flow rule, the conditional extremum method is proposed.

### 3.4 Conditional Extremum Methods Based on Cost Function (CE Methods)

In the process of deformation, the hardening and plastic deformation should affect each other. Therefore, the anisotropic parameters should be determined by both stresses and  $r$ -values, especially for materials with distortional hardening and evolution of  $r$ -values. For this, the stress cost function is constructed and different  $r$ -values are taken as constraint conditions. Then, the analytical solution of anisotropic parameters coupling the yield stresses and  $r$ -values can be obtained by solving the stationary point of the stress cost function. In this section, the anisotropic parameters calculated by different stress cost functions (based on different sets of experimental data of yield stresses) and constraint conditions are given and compared.

Constructing the following cost function with yield stresses,

$$\Phi = \sum_{i=1}^n \left[ \frac{1}{(\sigma_{z_i}^{pre})^2} - \frac{1}{(\sigma_{z_i}^{exp})^2} \right]^2 \quad (\text{Eq 34})$$

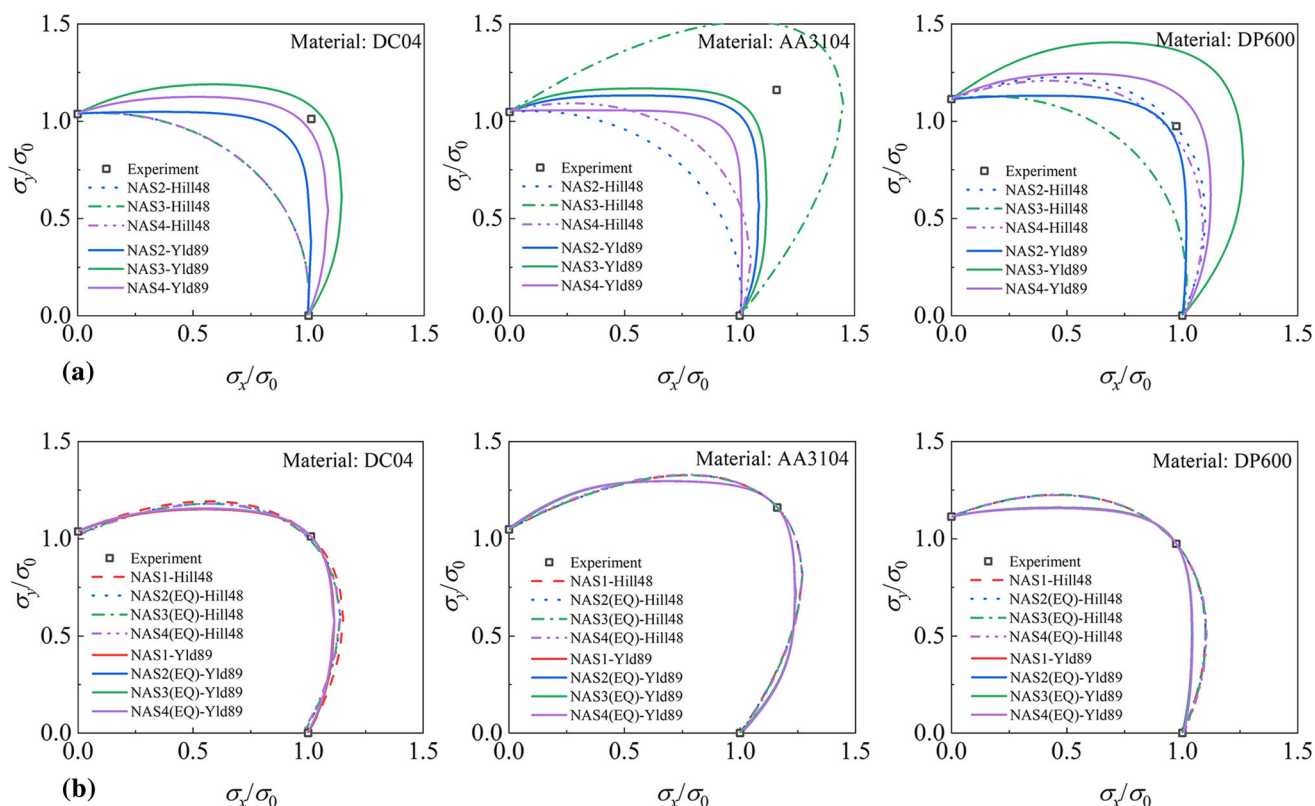


**Fig. 8** Yield loci predicted by different (a) NA methods (without equi-biaxial tensile stress) and (b) NA(EQ) methods (containing equi-biaxial tensile stress)

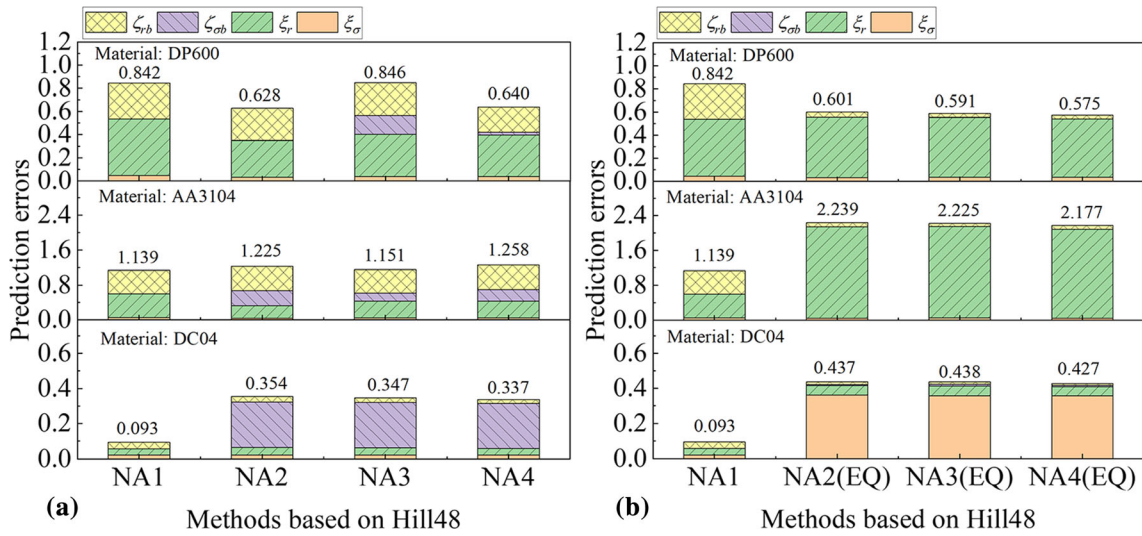


Fig. 9 Influence of the equi-biaxial tensile experimental data on the prediction errors of the Hill48 yield model

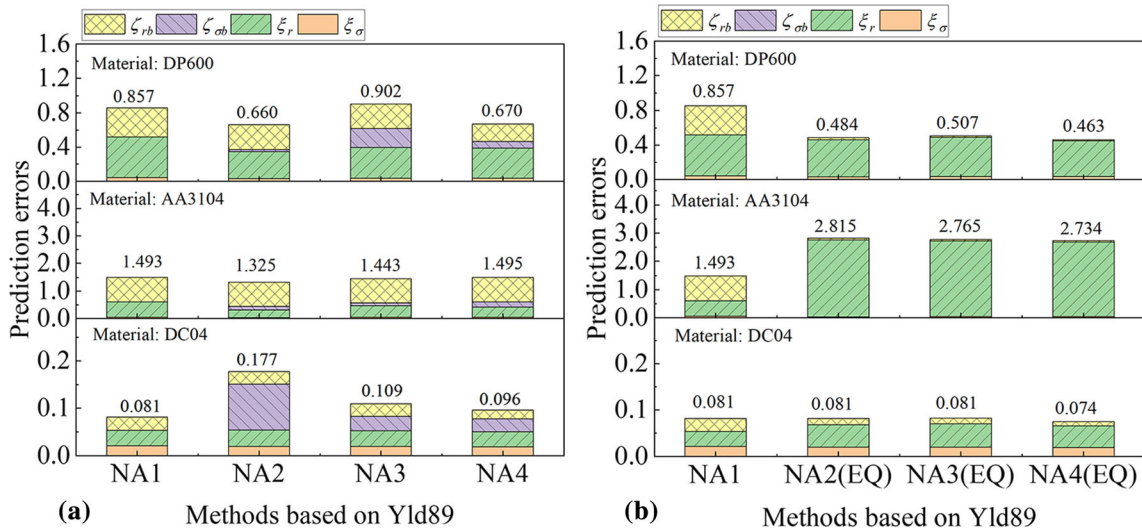


Fig. 10 Influence of the equi-biaxial tensile experimental data on the prediction errors of the Yld89 yield model

where  $\sigma_{\alpha}^{\text{exp}}$  and  $\sigma_{\alpha}^{\text{pre}}$  are the experimental uniaxial tensile yield stresses and the predicted value at orientation  $\alpha$  with respect to RD, respectively.

- (1) When  $n = 3$ ,  $\alpha_1 = 0$ ,  $\alpha_2 = 45$ , and  $\alpha_3 = 90$ . According to the Hill48 yield model and Eqs 4, 34 can be transformed as

$$\Phi = \left[ G + H - \frac{1}{(\sigma_0^{\text{exp}})^2} \right]^2 + \left[ \frac{F + G + 2N}{4} - \frac{1}{(\sigma_{45}^{\text{exp}})^2} \right]^2 + \left[ F + H - \frac{1}{(\sigma_{90}^{\text{exp}})^2} \right]^2 \quad (\text{Eq 35})$$

Taking  $r_0 = H/G$  and  $r_{90} = H/F$  as the constraint conditions, by taking the first derivative of  $\Phi$  with respect to  $H$  and  $N$ , the anisotropic parameters can be obtained as Eq. 36, which is named the CE1 method.

$$\begin{cases} H = \frac{1}{(1 + 1/r_0)^2 + (1 + 1/r_{90})^2} \left( \frac{1 + 1/r_0}{\sigma_0^2} + \frac{1 + 1/r_{90}}{\sigma_{90}^2} \right) \\ G = \frac{H}{r_0} \\ F = \frac{H}{r_{90}} \\ N = \frac{1}{2} (4/\sigma_{45}^2 - F - G) \end{cases} \quad (\text{Eq 36})$$

When taking  $r_0 = H/G$ ,  $r_{45} = N/(F + G) - 1/2$ , and  $r_{90} = H/F$  as the constraint conditions, by taking the first derivative of  $\Phi$  with respect to  $H$ , the anisotropic parameters can be obtained as Eq. 37, which is named the CE2 method.

$$\begin{cases} H = \frac{r_0^2 r_{90}^2 \left( \frac{1+1/r_0}{\sigma_0^2} + \frac{(1+r_{45})(1/r_0+1/r_{90})}{2\sigma_{45}^2} + \frac{1+1/r_{90}}{\sigma_{90}^2} \right)}{(1+r_0)^2 r_{90}^2 + (1+r_{45})^2 (r_0+r_{90})^2 / 4 + (1+r_{90})^2 r_0^2} \\ G = \frac{H}{r_0} \\ F = \frac{H}{r_{90}} \\ N = \frac{1}{2}(2r_{45} + 1)(F + G) \end{cases} \quad (\text{Eq 37})$$

(2) When  $n = 5$ ,  $\alpha_1 = 0$ ,  $\alpha_2 = 30$ ,  $\alpha_3 = 45$ ,  $\alpha_4 = 60$ , and  $\alpha_5 = 90$ . Taking  $r_0 = H/G$  and  $r_{90} = H/F$  as the constraint conditions, according to the above solution process, the anisotropic parameters are obtained as Eq. 38, which is named the CE3 method.

$$\begin{cases} H = \frac{A}{B} \\ G = \frac{H}{r_0} \\ F = \frac{H}{r_{90}} \\ N = \frac{16}{17} \left\{ \frac{3}{4} \left( \frac{1}{\sigma_{30}^2} + \frac{1}{\sigma_{60}^2} \right) + \frac{1}{\sigma_{45}^2} - \left[ \frac{23}{32} \left( \frac{1}{r_0} + \frac{1}{r_{90}} \right) + \frac{3}{8} \right] H \right\} \end{cases} \quad (\text{Eq 38})$$

where

$$\begin{aligned} A &= 2(1 + 1/r_0)/\sigma_0^2 + 2(1 + 1/r_{90})/\sigma_{90}^2 + (1/r_0 + 1/r_{90})/2\sigma_{45}^2 \\ &\quad + (9/r_0 + 1/r_{90} + 4)/8\sigma_{30}^2 + (1/r_0 + 9/r_{90} + 4)/8\sigma_{60}^2 \\ &\quad - \left[ \frac{23}{34} \left( \frac{1}{r_0} + \frac{1}{r_{90}} \right) + \frac{6}{17} \right] \left[ \frac{3}{4} \left( \frac{1}{\sigma_{30}^2} + \frac{1}{\sigma_{60}^2} \right) + \frac{1}{\sigma_{45}^2} \right] \\ B &= 2(1 + 1/r_0)^2 + 2(1 + 1/r_{90})^2 + (1/r_{90} + 1/r_0)^2 / 8 \\ &\quad + (1/r_{90} + 9/r_0 + 4)^2 / 128 + (9/r_{90} + 1/r_0 + 4)^2 / 128 \\ &\quad - \frac{16}{17} \left[ \frac{23}{32} (1/r_{90} + 1/r_0) + \frac{3}{8} \right]^2 \end{aligned}$$

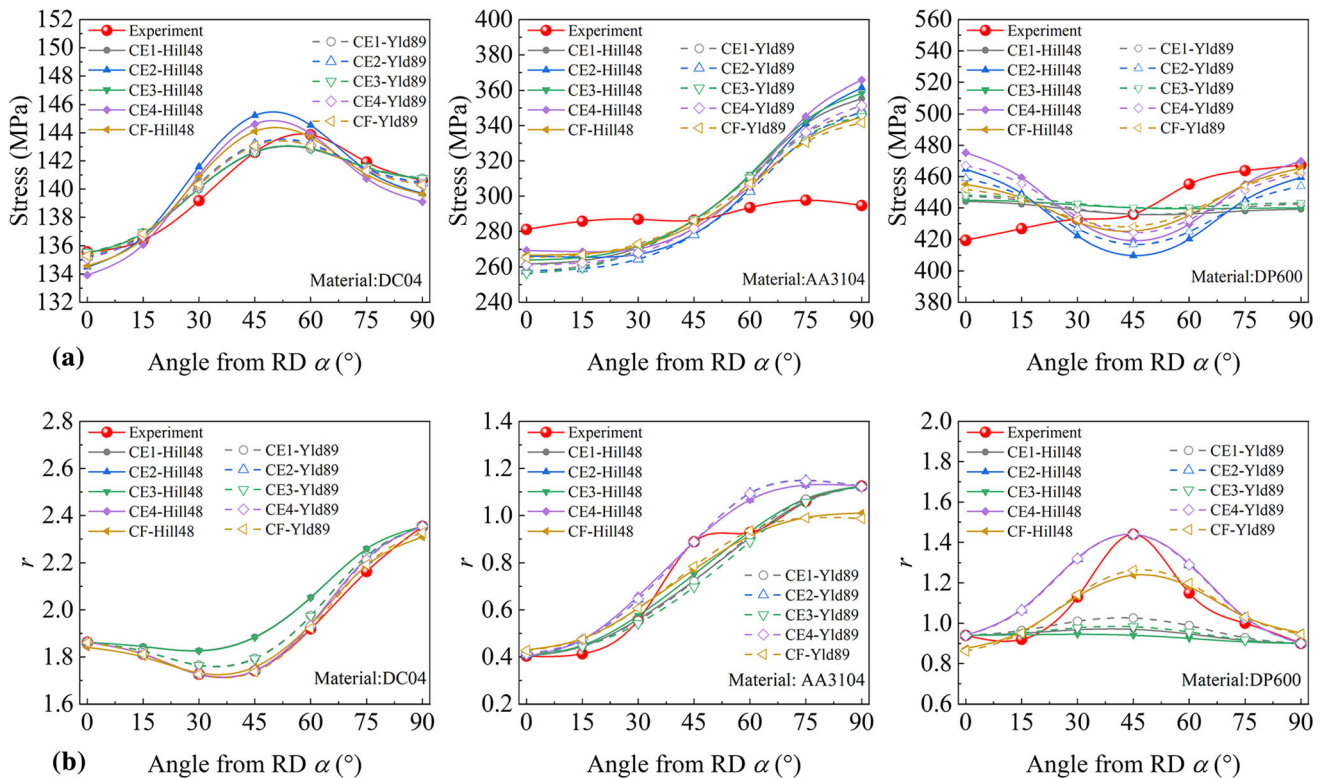


**Fig. 11** Comparison between experimental data and the results predicted by different CE methods (without equi-biaxial tensile experimental data): (a) Directional yield stresses; (b)  $r$ -values

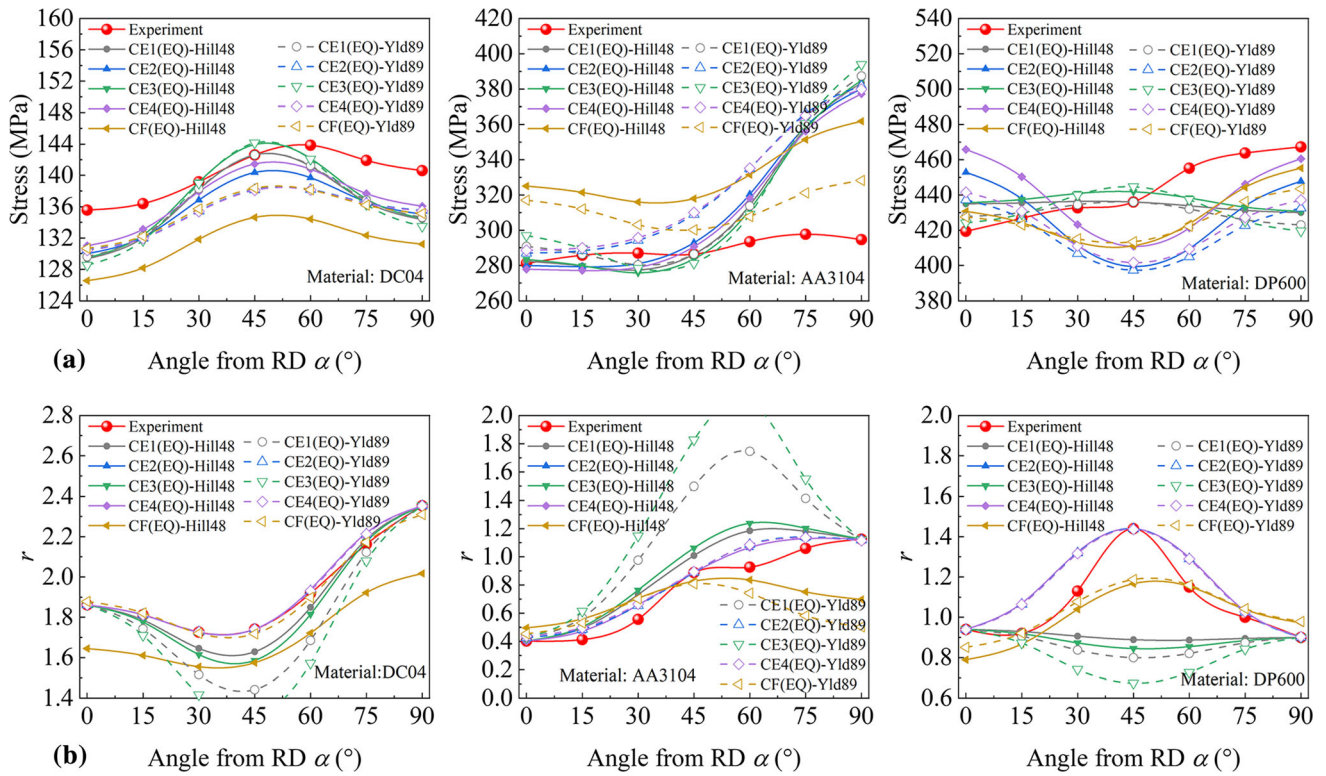


**Fig. 12** Comparison between experimental data and the results predicted by different CE(EQ) methods (containing equi-biaxial tensile experimental data): (a) Directional yield stresses; (b)  $r$ -values

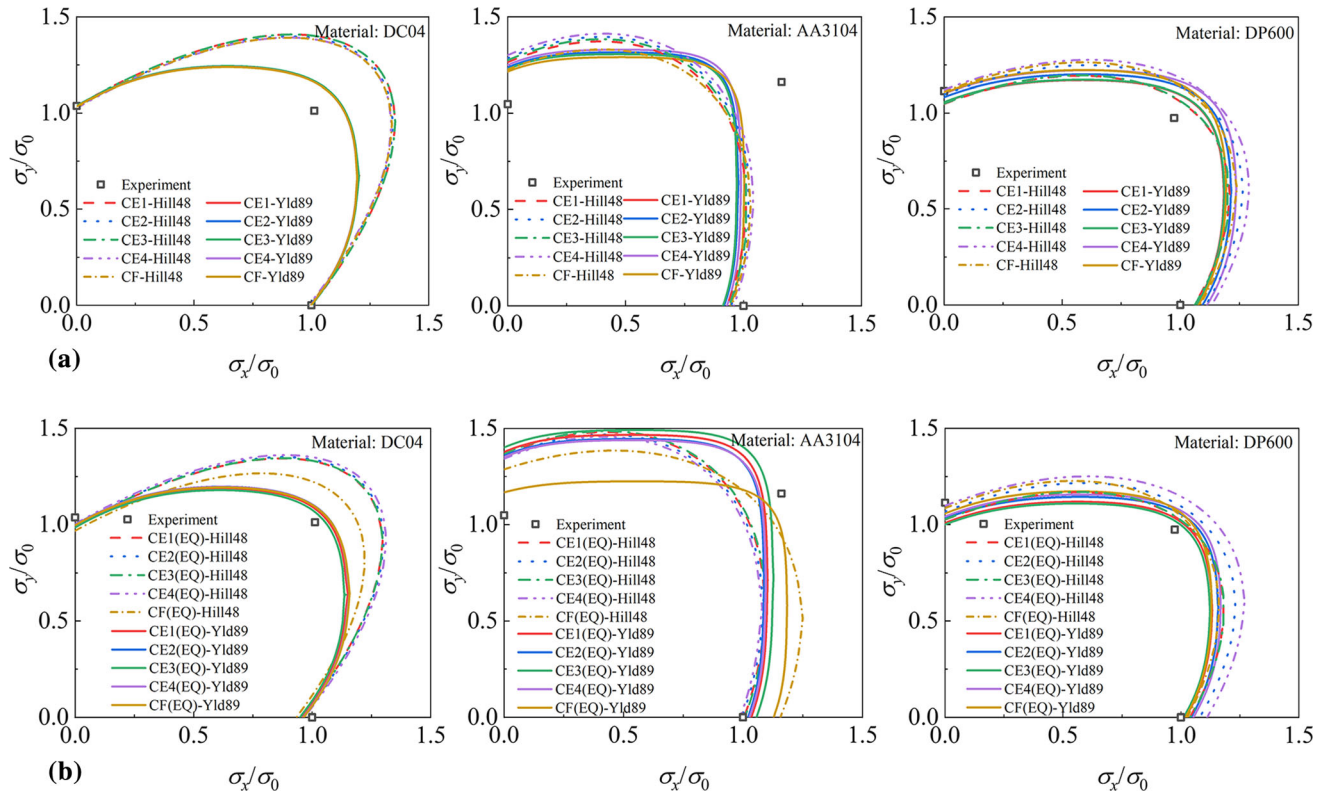


**Fig. 13** Yield loci predicted by different (a) CE methods (without equi-biaxial tensile stress) and (b) CE(EQ) methods (containing equi-biaxial tensile stress)

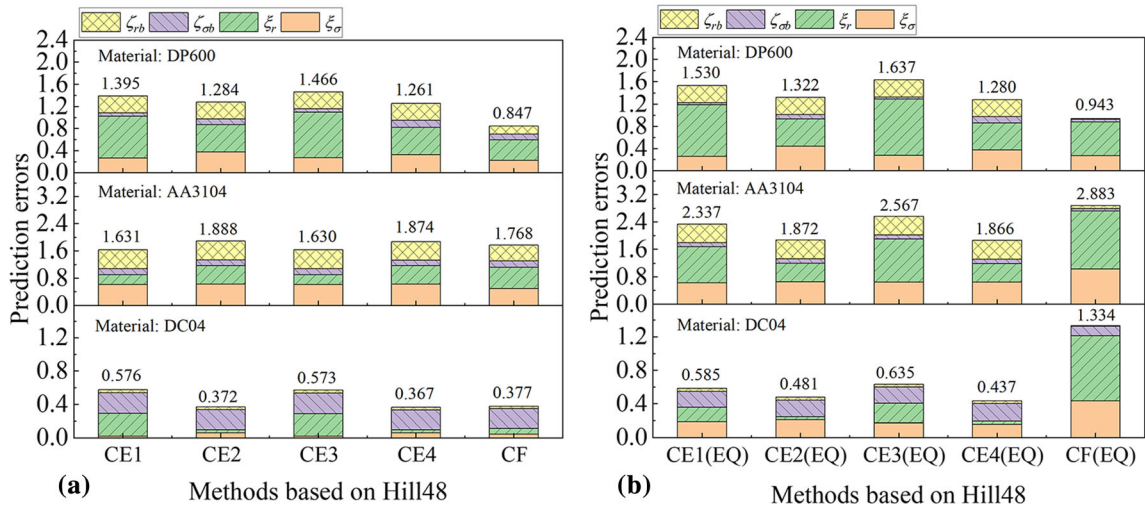


Fig. 14 Influence of the equi-biaxial tensile stress on the prediction errors of the Hill48 yield model

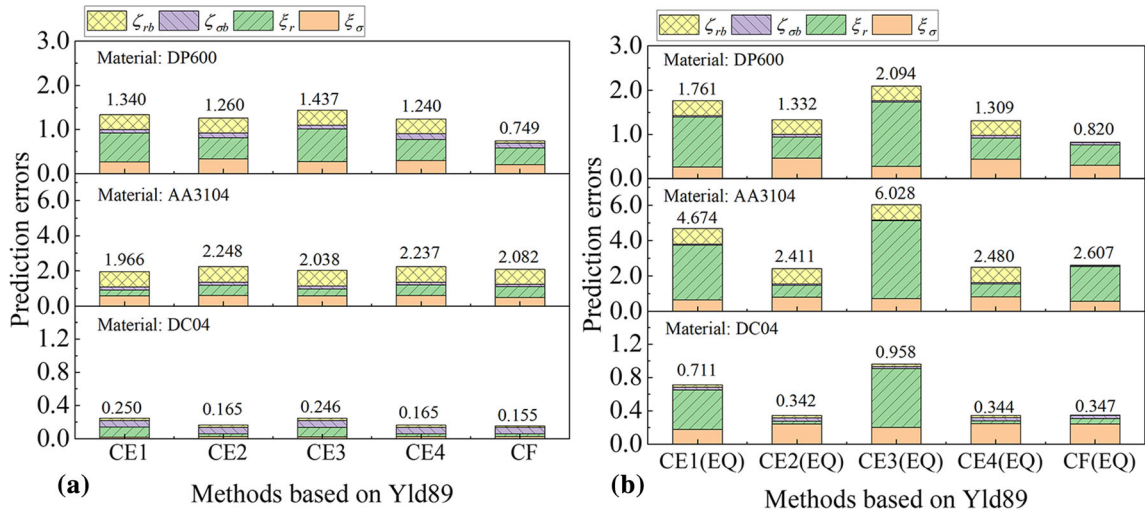


Fig. 15 Influence of the equi-biaxial tensile stress on the prediction errors of the Yld89 yield model

When taking  $r_0 = H/G$ ,  $r_{45} = N/(F + G) - 1/2$ , and  $r_{90} = H/F$  as the constraint conditions, the anisotropic parameters can be obtained as Eq. 39, which is named the CE4 method.

$$\begin{cases} H = \frac{B + C/\sigma_{45}^2 + D/\sigma_{30}^2 + E/\sigma_{60}^2}{A + C^2 + D^2 + E^2} \\ F = \frac{H}{r_{90}} \\ G = \frac{H}{r_0} \\ N = \frac{1}{2}(2r_{45} + 1)(F + G) \end{cases} \quad (\text{Eq 39})$$

where

$$\begin{aligned} A &= (1 + 1/r_0)^2 + (1 + 1/r_{90})^2, & B &= (1 + 1/r_0)/\sigma_0^2 + \\ & & & (1 + 1/r_{90})/\sigma_{90}^2, & C &= (1 + 1/r_{45})(1/r_0 + 1/r_{90})/2, \\ D &= [9/r_0 + 1/r_{90} + 4 + 3(2r_{45} + 1)(1/r_0 + 1/r_{90})]/16, \\ E &= [1/r_0 + 9/r_{90} + 4 + 3(2r_{45} + 1)(1/r_0 + 1/r_{90})]/16. \end{aligned}$$

- (3) To compare with the above methods, the following comprehensive cost function Eq. 40 with seven directional yield stresses and  $r$ -values is constructed. The anisotropic parameters can be obtained by minimizing the cost function, which is named the CF method.

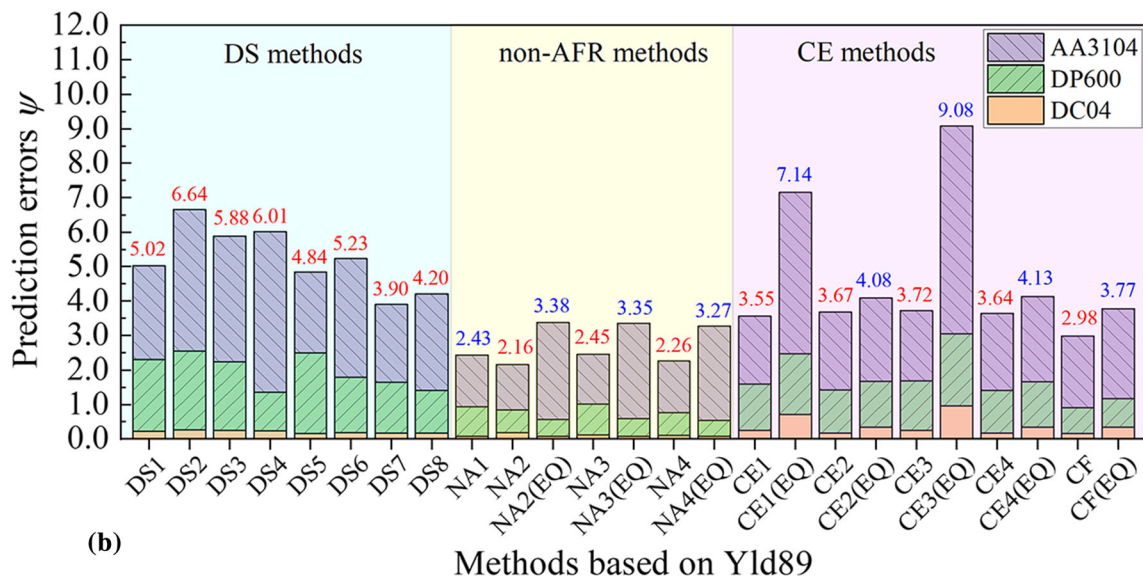
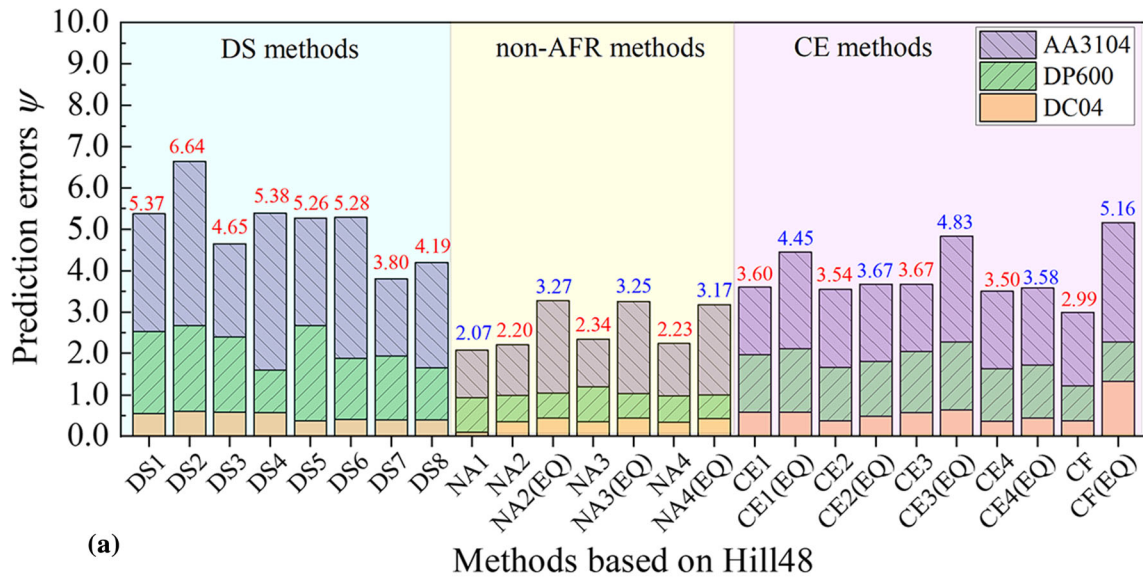
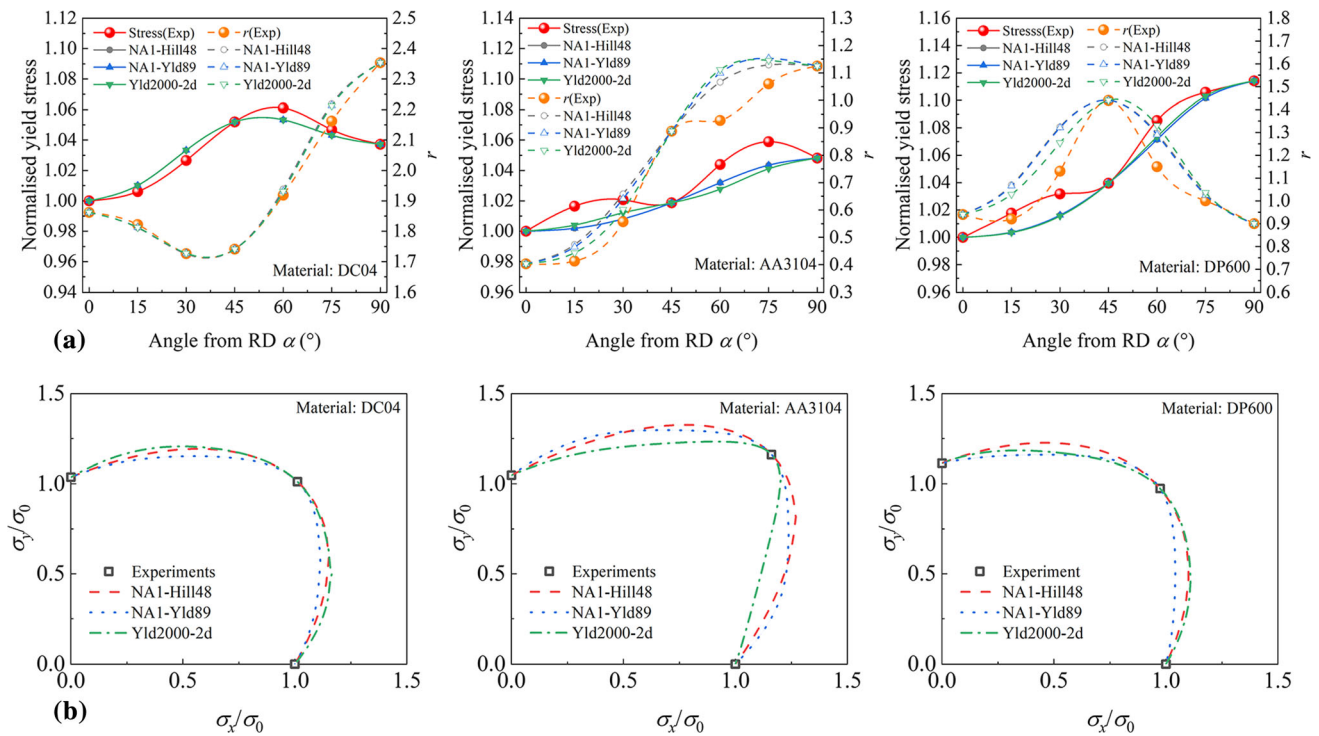


Fig. 16 Comparison of the prediction errors obtained by different methods

$$\Phi = \sum_{i=1}^7 \left[ \left( \frac{\sigma_{z_i}^{\text{exp}}}{\sigma_{z_i}^{\text{pre}}} - 1 \right)^2 \right] + \sum_{i=1}^7 \left[ \left( \frac{r_{z_i}^{\text{exp}}}{r_{z_i}^{\text{pre}}} - 1 \right)^2 \right] \quad (\text{Eq 40})$$

For the Yld89 yield model, its anisotropic parameters cannot be expressed explicitly. Therefore, the anisotropic parameters of different conditional extremum methods are solved numerically. The anisotropic parameters calculated by the above-mentioned CE methods are given in Appendix Table 6. Figure 11 shows the uniaxial tensile yield stress and  $r$ -value predicted by different CE methods based on the Hill48 yield model and Yld89 yield model. The constraint conditions have a higher effect on the predicted results than the cost function. The

cost function and constraint conditions will not change the predicted change law of the uniaxial tensile yield stresses and  $r$ -values. The difference between these CE methods is mainly reflected in the uniaxial tensile yield stress and  $r$ -value in the 45° direction. For the DC04 material, the CE2, CE4, and CF methods based on Hill48 can all give accurate prediction results. However, for DP600 and AA3104 materials, these CE methods can only approximately predict the  $r$ -values. The reason for this phenomenon is the limitations of the Hill48 model in predicting the directional yield stress and  $r$ -values. On the other hand, the anisotropic parameters of the Hill48 yield criterion are too few to contain more anisotropic characteristics. The same rule is also reflected in the prediction results of the Yld89 yield model. In contrast, for the DC04 material, CE



**Fig. 17** Comparison between the prediction results of the Hill48 and Yld89 yield models based on the NA1 method and that of the Yld2000-2d yield model: (a) Uniaxial tensile stress and  $r$ -value; (b) yield locus

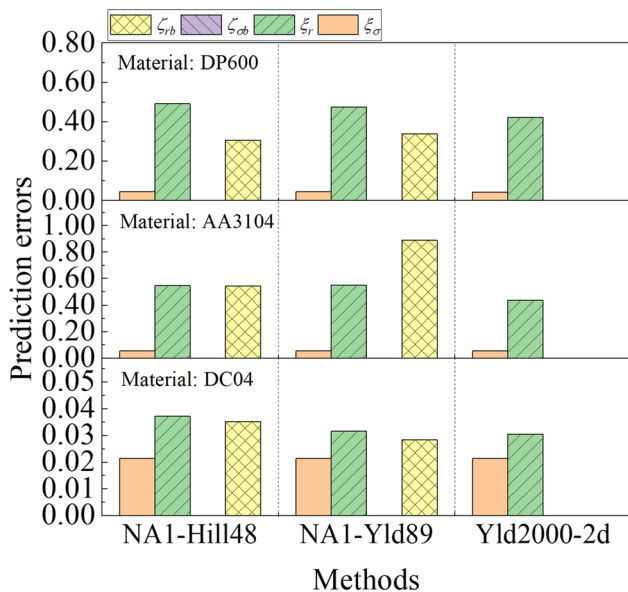


**Fig. 18** Prediction errors under different stress states obtained by different yield models

methods based on the Yld89 model are not sensitive to  $r_{45}$ . Whether  $r_{45}$  is included will not significantly change the predicted variation law of uniaxial tensile stress and the  $r$ -value

with angle. As shown in Fig. 13(a), the yield loci obtained by different CE methods are different but not significant. Because the Yld89 yield model has a higher-order equation form, the prediction accuracy of its yield loci is slightly higher than that of the Hill48 yield model, especially for DC04.

Similarly, the CE(EQ) method including equi-biaxial tensile stress can be obtained by adding the equi-biaxial tensile stress in the stress cost function. They are renamed CE1(EQ), CE2(EQ), CE3(EQ), and CE4(EQ). For the Hill48 yield model, the explicit solutions of the CE(EQ) methods can be easily obtained according to the above solution method, which is not repeated here. The anisotropic parameters of the Yld89 yield model are still solved numerically. The equi-biaxial tensile stress and  $r$ -value error term are added to Eq. 40, which is renamed the CF(EQ) method.

As shown in Figs. 12 and 13(b), the uniaxial tensile yield stresses,  $r$ -values and yield loci obtained by the CE(EQ) methods (considering equi-biaxial tensile stress) are given. The uniaxial tensile yield stress and  $r$ -value predicted by the CE(EQ) methods are different from those obtained by the CE methods, and the prediction errors of the uniaxial tensile stress state are increased. However, the prediction accuracy of equi-biaxial tensile stress is not significantly improved. This leads to an increase in the total prediction error of the CE(EQ) methods, as shown in Figs. 14 and 15. In addition, it can be seen that the predicted results of the Yld89 yield model are more sensitive to the equi-biaxial tensile stress than those of the Hill48 yield model.



## 4. Analysis of the Identification Strategy Results

The sum of prediction errors of the above three materials calculated by Eq 41 is shown in Fig. 16, which are used to evaluate the adaptability of the above identification strategies to different materials.

$$\Psi = \sum_{j=1}^3 (\xi_{\sigma} + \xi_r + \zeta_{\sigma b} + \zeta_{rb}) \quad (\text{Eq 41})$$

where  $j=1$  represents DC04 material,  $j=2$  represents DP600 material, and  $j=3$  represents AA3104 material.  $\xi_{\sigma}$  and  $\xi_r$  are the sum of prediction errors of the uniaxial tensile yield stresses and  $r$ -values at seven orientations, respectively.  $\zeta_{\sigma b}$  and  $\zeta_{rb}$  are the prediction errors of the equi-biaxial tensile yield stress and  $r$ -value, respectively.

As shown in Fig. 16, the sum of prediction errors obtained by the non-AFR methods is obviously less than that obtained with DS methods and CE methods. This is due to the advantages that the yield stress and deformation can be predicted with two sets of anisotropic parameters in the non-associated flow rule methods. Among the non-AFR methods, the prediction accuracy calculated by the NA1 method is the best. This indicates that when using the non-AFR method, the basic experimental data are sufficient. The prediction accuracy may not be effectively improved by adding additional uniaxial tensile test data to the error function. To further clarify the prediction accuracy of the NA methods, the comparison between the prediction results of the Hill48 and Yld89 yield models based on the NA1 method and those predicted by the advanced non-quadratic yield model Yld2000-2d is given. As shown in Fig. 17, the uniaxial tensile yield stress,  $r$ -value and equi-biaxial tensile stress obtained by the NA1 method can reach a prediction accuracy similar to that of the Yld2000-2d yield model. Their difference is mainly reflected in the equi-biaxial tensile  $r$ -value, as shown in Fig. 18. Therefore, the NA method can approximately substitute the higher-order yield model when the influence of the equi-biaxial tensile  $r$ -value on the simulation can be ignored.

Only one set of anisotropic parameters can be used under the associated flow rule, which presents a challenge when simultaneously describing the yield stress and  $r$ -value. Therefore, limited experimental data will inevitably lead to large prediction errors, such as the DS method. For this reason, including more experimental data on the anisotropic parameters is an effective way to solve this problem. The prediction accuracy obtained by the conditional extremum method proposed in this work is obviously better than that of the DS methods. Nevertheless, as far as the current research is concerned, the CE method is only good for low-carbon steel materials. There are still large errors in the prediction of high-strength steel and aluminum alloy. On the other hand, the increase in the input experimental data is only valid within a certain range. When the number of experimental data reaches saturation, the increase in experimental data will not significantly improve the prediction accuracy due to the limitations of the yield models.

In addition, the total prediction accuracy is not always improved by adding equi-biaxial tensile experimental data to the cost function of the NA methods and CE methods. In contrast, it will reduce the prediction accuracy of uniaxial tension. The prediction results of the Yld89 yield model also

show the same law. An important reason for this phenomenon is that the yield equation contains too few anisotropic parameters, which makes them unable to meet different stress states simultaneously. Therefore, when the number of anisotropic parameters of the yield equation is small, the premise of the reasonable application of the yield models is whether the variation form of yield stresses and  $r$ -values with angle conforms to the prediction form of the yield models.

## 5. Conclusions

The Hill48 yield model has inherent limitations in predicting uniaxial tensile yield stresses and  $r$ -values. There are two or three extreme points in the curve of uniaxial tensile yield stress changing with angle, which can only describe the materials whose stress distribution satisfies the form of monotonic increasing, monotonic decreasing, unimodal and single valley functions. The curve of  $r$ -values changing with angle has two to four extreme points, so it can only describe the materials that the distribution of  $r$ -value satisfies the form of monotonic increasing, monotonic decreasing, single peak, concave valley, coexist one peak and one valley. Therefore, the prediction accuracy of the Hill48 yield model depends on whether the anisotropic behavior of the material meets the above distribution law but is not directly related to the value of  $r$ .

The DS methods are unstable and greatly affected by material properties. The prediction errors obtained with the non-AFR methods are relatively minimal, and they have strong adaptability to different materials. To improve the prediction accuracy of the Hill48 yield model under the associated flow rule, this paper proposed a conditional extremum method. For materials that meet the characteristics of the Hill48 yield model, the CE2 method can obtain a prediction accuracy similar to that of the non-AFR method, and its analytical solution can be more conveniently applied to numerical simulation.

The increase in uniaxial tensile experimental data used in the cost function will not change the prediction law of directional yield stresses, and  $r$ -values and cannot significantly improve the prediction accuracy. In addition, the total prediction accuracy is not always improved by adding equi-biaxial tensile experimental data to the cost function of NA methods and CE methods. In contrast, the prediction accuracy of uniaxial tension will be reduced to varying degrees. Therefore, to further improve the prediction accuracy, we should focus on how to introduce new variables into the anisotropic parameters so that the yield function can contain more material properties.

## Acknowledgments

This work was supported by the National Natural Science Foundation of China [grant numbers 51975509, 52005431] and the Natural Science Foundation of Hebei Province [grant number E2020203086].

## Appendix

See Tables 3, 4, 5, 6

**Table 3 Anisotropic parameters obtained by different DS methods**

Materials		DS1	DS2	DS3	DS4	DS5	DS6	DS7	DS8
DC04	<i>H</i>	3.54E-05	3.55E-05	3.54E-05	3.55E-05	3.54E-05	3.55E-05	3.54E-05	3.55E-05
	<i>F</i>	1.52E-05	1.51E-05	1.5E-05	1.51E-05	1.52E-05	1.51E-05	1.5E-05	1.51E-05
	<i>G</i>	1.9E-05	1.89E-05	1.9E-05	1.91E-05	1.9E-05	1.89E-05	1.9E-05	1.91E-05
	<i>N</i>	8.12E-05	8.13E-05	8.13E-05	8.13E-05	7.66E-05	7.62E-05	7.63E-05	7.65E-05
	<i>a</i>	0.650	0.647	0.649	0.654	0.650	0.647	0.649	0.654
	<i>c</i>	1.350	1.353	1.351	1.363	1.350	1.353	1.351	1.363
	<i>h</i>	0.964	0.964	0.963	0.963	0.964	0.964	0.963	0.963
	<i>p</i>	0.944	0.944	0.944	0.943	0.938	0.936	0.937	0.937
	<i>m</i>	6.000	6.000	6.000	6.000	6.000	6.000	6.000	6.000
	DP600	<i>H</i>	2.75E-06	2.16E-06	2.75E-06	2.16E-06	2.75E-06	2.16E-06	2.75E-06
<i>F</i>		1.82E-06	2.41E-06	3.06E-06	2.41E-06	1.82E-06	2.41E-06	3.06E-06	2.41E-06
<i>G</i>		2.93E-06	3.52E-06	2.93E-06	2.30E-06	2.93E-06	3.51E-06	2.93E-06	2.30E-06
<i>N</i>		8.14E-06	7.56E-06	7.52E-06	8.16E-06	9.22E-06	1.14E-05	1.16E-05	9.15E-06
<i>a</i>		0.920	1.150	1.042	0.509	0.920	1.150	1.042	0.509
<i>c</i>		1.080	0.850	0.958	0.468	1.080	0.850	0.958	0.468
<i>h</i>		0.897	0.897	1.011	1.011	0.897	0.897	1.011	1.011
<i>p</i>		0.964	0.966	0.946	1.109	1.004	1.135	1.132	1.132
<i>m</i>		6.000	6.000	6.000	6.000	6.000	6.000	6.000	6.000
AA3104		<i>H</i>	3.63E-06	6.10E-06	3.63E-06	6.10E-06	3.63E-06	6.10E-06	3.63E-06
	<i>F</i>	7.88E-06	5.42E-06	3.23E-06	5.42E-06	7.88E-06	5.42E-06	3.23E-06	5.42E-06
	<i>G</i>	9.02E-06	6.55E-06	9.02E-06	1.51E-05	9.02E-06	6.55E-06	9.02E-06	1.51E-05
	<i>N</i>	1.59E-05	1.84E-05	1.83E-05	1.41E-05	2.35E-05	1.66E-05	1.70E-05	2.85E-05
	<i>a</i>	1.398	0.990	1.220	9.664	1.398	0.990	1.220	9.664
	<i>c</i>	0.602	1.010	0.780	6.178	0.602	1.010	0.780	6.178
	<i>h</i>	0.954	0.954	0.737	0.737	0.954	0.954	0.737	0.737
	<i>p</i>	0.984	0.983	1.015	0.686	1.129	0.951	0.940	0.940
	<i>m</i>	8.000	8.000	8.000	8.000	8.000	8.000	8.000	8.000

**Table 4 Anisotropic parameters based on stresses**

Materials		NAS1	NAS2	NAS2(EQ)	NAS3	NAS3(EQ)	NAS4	NAS4(EQ)
DC04	<i>F<sub>σ</sub></i>	1.96E-05	4.56E-05	2.47E-05	4.57E-05	2.49E-05	4.56E-05	2.47E-05
	<i>G<sub>σ</sub></i>	2.34E-05	4.99E-05	2.47E-05	4.99E-05	2.49E-05	4.99E-05	2.47E-05
	<i>H<sub>σ</sub></i>	3.09E-05	4.68E-06	2.47E-05	4.63E-06	2.49E-05	4.75E-06	2.47E-05
	<i>N<sub>σ</sub></i>	7.68E-05	4.99E-05	2.47E-05	4.99E-05	2.49E-05	4.99E-05	2.47E-05
	<i>a<sub>σ</sub></i>	1.033	1.932	1.049	0.875	1.048	1.242	1.052
	<i>c<sub>σ</sub></i>	0.967	0.103	0.987	1.160	0.985	0.801	0.992
	<i>h<sub>σ</sub></i>	0.964	0.959	0.959	0.959	0.959	0.958	0.958
	<i>p<sub>σ</sub></i>	0.939	0.917	0.935	0.938	0.936	0.932	0.935
	<i>m</i>	6.000	6.000	6.000	6.000	6.000	6.000	6.000
	DP600	<i>F<sub>σ</sub></i>	2.44E-06	2.46E-06	2.45E-06	3.75E-06	2.45E-06	2.62E-06
<i>G<sub>σ</sub></i>		3.55E-06	3.55E-06	2.45E-06	4.83E-06	2.45E-06	3.67E-06	2.47E-06
<i>H<sub>σ</sub></i>		2.13E-06	2.11E-06	2.45E-06	8.20E-07	2.45E-06	1.94E-06	2.47E-06
<i>N<sub>σ</sub></i>		7.52E-06	7.13E-06	2.45E-06	6.02E-06	2.45E-06	7.15E-06	2.47E-06
<i>a<sub>σ</sub></i>		1.541	1.788	1.538	0.469	1.537	0.968	1.524
<i>c<sub>σ</sub></i>		0.459	0.201	0.453	1.504	0.438	0.955	0.399
<i>h<sub>σ</sub></i>		0.897	0.899	0.899	0.899	0.898	0.902	0.902
<i>p<sub>σ</sub></i>		0.969	0.940	0.941	0.954	0.957	0.960	0.962
<i>m</i>		6.000	6.000	6.000	6.000	6.000	6.000	6.000
AA3104		<i>F<sub>σ</sub></i>	4.11E-06	1.04E-05	4.12E-06	2.83E-06	4.14E-06	8.26E-06
	<i>G<sub>σ</sub></i>	5.25E-06	1.15E-05	4.12E-06	3.94E-06	4.14E-06	9.38E-06	4.12E-06
	<i>H<sub>σ</sub></i>	7.39E-06	1.13E-06	4.12E-06	8.66E-06	4.14E-06	3.11E-06	4.12E-06
	<i>N<sub>σ</sub></i>	1.96E-05	1.27E-05	4.12E-06	2.06E-05	4.14E-06	1.51E-05	4.12E-06
	<i>a<sub>σ</sub></i>	0.358	1.062	0.357	0.825	0.358	1.877	0.357
	<i>c<sub>σ</sub></i>	1.642	0.934	1.638	1.150	1.621	0.020	1.539
	<i>h<sub>σ</sub></i>	0.954	0.955	0.955	0.954	0.954	0.954	0.954
	<i>p<sub>σ</sub></i>	0.982	0.962	0.965	0.974	0.974	0.981	0.979
	<i>m</i>	8.000	8.000	8.000	8.000	8.000	8.000	8.000

**Table 5 Anisotropic parameters based on *r*-values**

Materials		NAR1	NAR2	NAR2(EQ)	NAR3	NAR3(EQ)	NAR4	NAR4(EQ)
DC04	<i>F<sub>r</sub></i>	0.276	1.723	1.744	1.912	1.695	1.540	1.687
	<i>G<sub>r</sub></i>	0.349	2.171	2.159	2.397	2.102	1.923	2.079
	<i>H<sub>r</sub></i>	0.650	4.051	4.064	4.482	3.958	3.584	3.916
	<i>N<sub>r</sub></i>	1.402	8.668	8.696	9.632	8.484	7.730	8.425
	<i>a<sub>r</sub></i>	0.649	0.809	0.862	0.661	0.856	0.720	0.666
	<i>c<sub>r</sub></i>	1.351	1.685	1.802	1.378	1.788	1.493	1.385
	<i>h<sub>r</sub></i>	0.963	0.963	0.965	0.963	0.966	0.964	0.966
	<i>p<sub>r</sub></i>	0.937	0.935	0.936	0.936	0.936	0.937	0.938
	<i>m</i>	6.000	6.000	6.000	6.000	6.000	6.000	6.000
	DP600	<i>F<sub>r</sub></i>	0.538	2.848	3.728	2.438	2.320	2.499
<i>G<sub>r</sub></i>		0.515	2.784	4.467	2.381	2.798	2.561	2.866
<i>H<sub>r</sub></i>		0.484	2.590	3.703	2.169	2.261	2.227	2.261
<i>N<sub>r</sub></i>		2.044	9.651	14.041	8.786	9.330	9.212	9.518
<i>a<sub>r</sub></i>		1.042	1.355	1.671	1.827	1.893	1.220	1.476
<i>c<sub>r</sub></i>		0.958	1.246	1.520	1.644	1.683	1.074	1.287
<i>h<sub>r</sub></i>		1.011	1.005	0.967	1.005	0.966	0.994	0.966
<i>p<sub>r</sub></i>		1.132	1.077	1.060	1.109	1.092	1.109	1.096
<i>m</i>		6.000	6.000	6.000	6.000	6.000	6.000	6.000
AA3104		<i>F<sub>r</sub></i>	0.255	2.004	3.135	1.860	2.874	1.713
	<i>G<sub>r</sub></i>	0.712	5.732	4.439	5.171	3.989	4.962	4.836
	<i>H<sub>r</sub></i>	0.287	2.262	2.949	2.070	2.638	1.885	3.126
	<i>N<sub>r</sub></i>	1.343	9.590	9.363	9.170	8.982	8.681	10.817
	<i>a<sub>r</sub></i>	1.220	1.494	1.798	1.627	0.665	1.602	1.415
	<i>c<sub>r</sub></i>	0.780	0.957	1.423	1.045	0.517	1.001	1.084
	<i>h<sub>r</sub></i>	0.737	0.737	0.963	0.744	0.964	0.737	0.963
	<i>p<sub>r</sub></i>	0.940	0.904	0.967	0.922	0.990	0.922	0.992
	<i>m</i>	8.000	8.000	8.000	8.000	8.000	8.000	8.000

**Table 6 Anisotropic parameters based on the CE methods**

Materials		CE1	CE1(EQ)	CE2	CE2(EQ)	CE3	CE3(EQ)	CE4	CE4(EQ)	CF	CF(EQ)
DC04	<i>F</i>	1.51E-05	1.65E-05	1.53E-05	1.64E-05	1.51E-05	1.65E-05	1.54E-05	1.61E-05	1.55E-05	1.92E-05
	<i>G</i>	1.90E-05	2.09E-05	1.93E-05	2.07E-05	1.90E-05	2.08E-05	1.95E-05	2.04E-05	1.94E-05	2.36E-05
	<i>H</i>	3.54E-05	3.89E-05	3.60E-05	3.85E-05	3.54E-05	3.88E-05	3.63E-05	3.79E-05	3.58E-05	3.88E-05
	<i>N</i>	8.13E-05	7.96E-05	7.75E-05	8.30E-05	8.12E-05	7.79E-05	7.82E-05	8.17E-05	7.89E-05	8.89E-05
	<i>a</i>	0.650	0.849	0.659	0.816	0.650	0.893	0.662	0.818	0.659	0.811
	<i>c</i>	1.354	1.770	1.373	1.700	1.354	1.861	1.379	1.705	1.366	1.683
	<i>h</i>	0.963	0.963	0.963	0.963	0.963	0.963	0.963	0.963	0.964	0.967
	<i>p</i>	0.944	0.893	0.937	0.937	0.944	0.872	0.937	0.937	0.938	0.936
	<i>m</i>	6.000	6.000	6.000	6.000	6.000	6.000	6.000	6.000	6.000	6.000
	DP600	<i>F</i>	2.73E-06	2.85E-06	2.49E-06	2.62E-06	2.72E-06	2.84E-06	2.38E-06	2.48E-06	2.37E-06
<i>G</i>		2.61E-06	2.72E-06	2.39E-06	2.51E-06	2.60E-06	2.72E-06	2.28E-06	2.38E-06	2.58E-06	3.01E-06
<i>H</i>		2.46E-06	2.56E-06	2.24E-06	2.36E-06	2.45E-06	2.55E-06	2.15E-06	2.23E-06	2.25E-06	2.38E-06
<i>N</i>		7.85E-06	7.74E-06	9.47E-06	9.97E-06	7.66E-06	7.47E-06	9.05E-06	9.42E-06	8.59E-06	9.10E-06
<i>a</i>		0.706	0.926	0.607	0.811	0.699	0.974	0.546	0.765	0.671	0.933
<i>c</i>		0.649	0.852	0.558	0.746	0.643	0.896	0.502	0.704	0.606	0.850
<i>h</i>		1.011	1.011	1.011	1.011	1.011	1.011	1.011	1.010	0.976	0.964
<i>p</i>		1.034	0.972	1.131	1.131	1.022	0.935	1.131	1.130	1.078	1.051
<i>m</i>		6.000	6.000	6.000	6.000	6.000	6.000	6.000	6.000	6.000	6.000
AA3104		<i>F</i>	3.73E-06	3.20E-06	3.60E-06	3.26E-06	3.66E-06	3.18E-06	3.52E-06	3.31E-06	4.18E-06
	<i>G</i>	1.04E-05	8.93E-06	1.01E-05	9.09E-06	1.02E-05	8.87E-06	9.82E-06	9.23E-06	9.83E-06	6.33E-06
	<i>H</i>	4.19E-06	3.60E-06	4.05E-06	3.66E-06	4.12E-06	3.57E-06	3.96E-06	3.72E-06	4.22E-06	3.14E-06
	<i>N</i>	1.73E-05	1.83E-05	1.90E-05	1.71E-05	1.74E-05	1.88E-05	1.85E-05	1.74E-05	1.78E-05	1.44E-05
	<i>a</i>	2.442	0.920	2.430	1.022	2.528	0.778	2.188	0.972	1.953	0.517
	<i>c</i>	1.576	0.605	1.568	0.674	1.637	0.515	1.417	0.650	1.226	0.248
	<i>h</i>	0.741	0.751	0.741	0.752	0.743	0.754	0.743	0.760	0.777	0.966
	<i>p</i>	0.902	1.058	0.941	0.942	0.896	1.109	0.941	0.944	0.937	1.090
	<i>m</i>	8.000	8.000	8.000	8.000	8.000	8.000	8.000	8.000	8.000	8.000

## References

1. R.Hill, A Theory of the Yielding and Plastic Flow of Anisotropic Metals, *Proc. R. Soc. Lond. Ser. A Math. Phys. Sci.*, 1948, **193**, p 281–297
2. F.Barlat and K.Lian, Plastic Behavior and Stretchability of Sheet Metals. Part I: A Yield Function for Orthotropic Sheets Under Plane Stress Conditions, *Int. J. Plast.*, 1989, **5**, p 51–66
3. W.F. Hosford, A Generalized Isotropic Yield Criterion, *J. Appl. Mech. Trans. ASME*, 1972, **39**(2), p 607–609
4. F. Barlat, D.J. Lege and J.C. Brem, A Six-Component Yield Function for Anisotropic Materials, *Int. J. Plast.*, 1991, **7**(7), p 693–712
5. F. Barlat, J. Brem, J.W. Yoon, K. Chung, R. Dick, D. Lege et al., Plane Stress Yield Function for Aluminum Alloy Sheets—Part 1: Theory, *Int. J. Plast.*, 2003, **19**, p 1297–1319
6. F. Barlat, H. Aretz, J.W. Yoon, M.E. Karabin, J.C. Brem and R.E. Dick, Linear Transformation-Based Anisotropic Yield Functions, *Int. J. Plast.*, 2005, **21**(5), p 1009–1039
7. O. Cazacu, B. Plunkett and F. Barlat, Orthotropic Yield Criterion for Hexagonal Closed Packed Metals, *Int. J. Plast.*, 2006, **22**(7), p 1171–1194
8. W. Hu, Constitutive Modeling of Orthotropic Sheet Metals by Presenting Hardening-Induced Anisotropy, *Int. J. Plast.*, 2007, **23**(4), p 620–639
9. M. Koç, Y. Aue-U-Lan and T. Altan, On the Characteristics of Tubular Materials for Hydroforming - Experimentation and Analysis, *Int. J. Mach. Tools Manuf.*, 2001, **41**(5), p 761–772
10. H.B. Wang, M. Wan, X.D. Wu and Y. Yan, Subsequent Yield Loci of Aluminum Alloy Sheet, *Trans. Nonferrous Met. Soc. China*, 2009, **19**(5), p 1076–1080
11. R.E. Dick and J.W. Yoon, Plastic Anisotropy and Failure in Thin Metal: Material Characterization and Fracture Prediction with an Advanced Constitutive Model and Polar EPS (Effective Plastic Strain) Fracture Diagram for AA 3014–H19, *Int. J. Solids Struct.*, 2018, **151**, p 195–213
12. N. Tardif and S. Kyriakides, Determination of Anisotropy and Material Hardening for Aluminum Sheet Metal, *Int. J. Solids Struct.*, 2012, **49**(25), p 3496–3506
13. M.S. Aydin, J. Gerlach, L. Kessler and A.E. Tekkaya, Yield Locus Evolution and Constitutive Parameter Identification Using Plane Strain Tension and Tensile Tests, *J. Mater. Process. Technol.*, 2011, **211**(12), p 1957–1964
14. F. Bron and J. Besson, A Yield Function for Anisotropic Materials Application to Aluminum Alloys, *Int. J. Plast.*, 2004, **20**(4–5), p 937–963
15. D. Banabic, H. Aretz, D.S. Comsa and L. Paraianu, An Improved Analytical Description of Orthotropy in Metallic Sheets, *Int. J. Plast.*, 2005, **21**(3), p 493–512
16. F. Grytten, B. Holmedal, O.S. Hopperstad and T. Børvik, Evaluation of Identification Methods for YLD2004-18p, *Int. J. Plast.*, 2008, **24**(12), p 2248–2277
17. J. Zhu, S.Y. Huang, W. Liu, J.H. Hu and X.F. Zou, Calibration of Anisotropic Yield Function by Introducing Plane Strain Test Instead of Equi-Biaxial Tensile Test, *Trans. Nonferrous Met. Soc. China*, 2018, **28**(11), p 2307–2313
18. A. Khalfallah, J.L. Alves, M.C. Oliveira and L.F. Menezes, Influence of the Characteristics of the Experimental Data Set Used to Identify Anisotropy Parameters, *Simul. Model. Pract. Theory*, 2015, **53**, p 15–44
19. B. Tang and Y. Lou, Effect of Anisotropic Yield Functions on the Accuracy of Material Flow and Its Experimental Verification, *Acta Mech. Solida Sin.*, 2019, **32**(1), p 50–68
20. A. Khalfallah, M.C. Oliveira, J.L. Alves, T. Zribi, H. Belhadjalah and L.F. Menezes, Mechanical Characterization and Constitutive Parameter Identification of Anisotropic Tubular Materials for Hydroforming Applications, *Int. J. Mech. Sci.*, 2015, **104**, p 91–103
21. K. Hariharan, N.T. Nguyen, N. Chakraborti, F. Barlat and M.G. Lee, Determination of Anisotropic Yield Coefficients by a Data-Driven Multiobjective Evolutionary and Genetic Algorithm, *Mater. Manuf. Process.*, 2015, **30**(4), p 403–413
22. K. Bandyopadhyay, K. Hariharan, M.G. Lee and Q. Zhang, Robust Multi Objective Optimization of Anisotropic Yield Function Coefficients, *Mater. Des.*, 2018, **156**, p 184–197
23. É. Markiewicz, B. Langrand and D. Notta-Cuvier, A Review of Characterisation and Parameters Identification of Materials Constitutive and Damage Models: From Normalised Direct Approach to Most Advanced Inverse Problem Resolution, *Int. J. Impact Eng.*, 2017, **110**, p 371–381
24. A. Güner, C. Soyarslan, A. Brosius and A.E. Tekkaya, Characterization of Anisotropy of Sheet Metals Employing Inhomogeneous Strain Fields for Yld 2000–2D Yield Function, *Int. J. Solids Struct.*, 2012, **49**(25), p 3517–3527
25. M. Teaca, I. Charpentier, M. Martiny and G. Ferron, Identification of Sheet Metal Plastic Anisotropy Using Heterogeneous Biaxial Tensile Tests, *Int. J. Mech. Sci.*, 2010, **52**(4), p 572–580
26. N. Souto, A. Andrade-Campos and S. Thuillier, Mechanical Design of a Heterogeneous Test for Material Parameters Identification, *Int. J. Mater. Form.*, 2017, **10**(3), p 353–367
27. M. Grédiac and F. Pierron, Applying the Virtual Fields Method to the Identification of Elasto-Plastic Constitutive Parameters, *Int. J. Plast.*, 2006, **22**(4), p 602–627
28. F. Pierron, S. Avril and V.T. Tran, Extension of the Virtual Fields Method to Elasto-Plastic Material Identification with Cyclic Loads and Kinematic Hardening, *Int. J. Solids Struct.*, 2010, **47**(22–23), p 2993–3010
29. M. Rossi and F. Pierron, Identification of Plastic Constitutive Parameters at Large Deformations from Three Dimensional Displacement Fields, *Comput. Mech.*, 2012, **49**(1), p 53–71
30. M. Rossi, F. Pierron and M. Štamborská, Application of the Virtual Fields Method to Large Strain Anisotropic Plasticity, *Int. J. Solids Struct.*, 2016, **97–98**, p 322–335
31. M. Rossi and F. Pierron, On the Use of Simulated Experiments in Designing Tests for Material Characterization from Full-Field Measurements, *Int. J. Solids Struct.*, 2012, **49**(3–4), p 420–435
32. J.H. Kim, F. Barlat, F. Pierron and M.G. Lee, Determination of Anisotropic Plastic Constitutive Parameters Using the Virtual Fields Method, *Exp. Mech.*, 2014, **54**(7), p 1189–1204
33. J.M.P. Martins, A. Andrade-Campos and S. Thuillier, Calibration of Anisotropic Plasticity Models Using a Biaxial Test and the Virtual Fields Method, *Int. J. Solids Struct.*, 2019, **172–173**, p 21–37
34. S. Zhang, L. Leotoing, D. Guines, S. Thuillier and S.L. Zang, Calibration of Anisotropic Yield Criterion with Conventional Tests or Biaxial Test, *Int. J. Mech. Sci.*, 2014, **85**, p 142–151
35. J. Fu, W. Xie, J. Zhou and L. Qi, A Method for the Simultaneous Identification of Anisotropic Yield and Hardening Constitutive Parameters for Sheet Metal Forming, *Int. J. Mech. Sci.*, 2020, **181**, p 105756

**Publisher's Note** Springer Nature remains neutral with regard to jurisdictional claims in published maps and institutional affiliations.